Observation of geometric and dynamical phases by neutron interferometry

B. E. Allman,* H. Kaiser, and S. A. Werner
Research Reactor Center and Physics Department, University of Missouri–Columbia, Columbia, Missouri 65211

A. G. Wagh† and V. C. Rakhecha†
Solid State Physics Division, Bhabha Atomic Research Center, Mumbai 400085, India

J. Summhammer
Atominstitut der Österreichischen Universitäten, Schüttelstrasse 115, A-1020 Wien, Austria
(Received 9 April 1997)

The total phase acquired during an evolution of a quantal system has two components: the usual dynamical phase, $-1/\hbar \int H(t)dt$, given by the integrated expectation value of the Hamiltonian, and a geometric phase $\Phi_G(C)$ which depends only on the geometry of the curve traced in ray space. We have performed an interference experiment using polarized neutrons which clearly demarcates the separate contributions of the dynamical and geometric phases to the total. In the experiment, the two phases arise from two distinct physical operations, a translation and a rotation of a spin flipper within the interferometer, respectively. This work also constitutes the first direct observation of the Pauli anticommutation; a purely geometric phase shift of π radians appears after a reversal of the current in one of the spin flippers. The experiment was carried out at the 10 MW University of Missouri Research Reactor using a skew-symmetric perfect-silicon-crystal neutron interferometer. A detailed description of the experiment and its interpretation is given in this paper. [S1050-2947(97)03911-5]

PACS number(s): 03.65.Bz, 42.25.Hz, 42.25.Ja

I. INTRODUCTION

The concept of geometric phase has been of increasing interest and activity since Berry's inspired discovery in 1983 [1]. While considering the behavior of quantum-mechanical systems, Berry found that, for a Hamiltonian, slowly cycled in time T, along a curve C of external parameters, an initial eigenstate with the energy eigenvalue $E(t)$ returns to the original state, in the adiabatic approximation, multiplied by two phase factors, prescribed by

$$|\Psi(T)\rangle = \exp\left\{\frac{-1}{\hbar}\int_T E(t)dt\right\}\exp\{i\Phi_G(C)\}|\Psi(0)\rangle. \tag{1}$$

The first phase factor is the standard, Hamiltonian-dependent dynamical phase. The second is a nonintegrable, path-dependent phase, which he termed the ''geometric phase.'' This phase is truly geometric, as it is independent of the rate, the Hamiltonian, and the energy eigenstate, and depends exclusively on the geometry of the curve traced in ray space. Such phase shifts of geometric origin were already included in the standard formulations of quantum mechanics, e.g., the topological Aharonov-Bohm effects, but their true geometric nature has only been appreciated recently.

Historically, however, the geometric phase was first observed by Pancharatnam in his study of the interference of polarized light [2]. By considering three nonorthogonal states of polarization represented by three points on the Poincaré sphere, he found that if the first and second states are ''in phase'' (a condition defined as a maximum in their interfered intensity), and the second and third states are ''in phase,'' then the first and third states are not necessarily in phase. Pancharatnam showed that the excess phase of the third state over the first is minus half the solid angle subtended by the spherical triangle formed by the three states at the center of the Poincaré sphere. The ideas of Pancharatnam have since been used to obtain geometric phase [3,4], arising in completely general evolutions.

Following its discovery, the geometric phase has been generalized and found to occur even when the evolution is nonadiabatic [5], noncyclic [3], and nonunitary [3]. For a parallel transported quantum state, the geometric phase is a consequence of the curvature of the connection (a rule permitting the comparison of their phases) between two neighboring rays. Moreover, the geometric phase represents an example of anholonomy in that the parallel transported quantal system fails to return to its original value when altered around a cycle, and is thus nonintegrable. A completely general expression in terms of just the state density operator for the geometric phase brings out its exclusive dependence on the ray space geometry [4].

The geometric phase has been observed in a broad spectrum of physical phenomenon from classical [6] to quantum physics [7–16]. In early experiments to observe the geometric phase, an adiabatic evolution was employed, via spin precession in various magnetic-field configurations [12,13]. Unfortunately, this generates a dynamical phase background which is generally much larger than the geometric component. Therefore, an ideal experiment should not effect an

*Present address: School of Physics, University of Melbourne, Parkville, Australia 3052.
†Electronic address: sspd@magnum.barctl.ernet.in

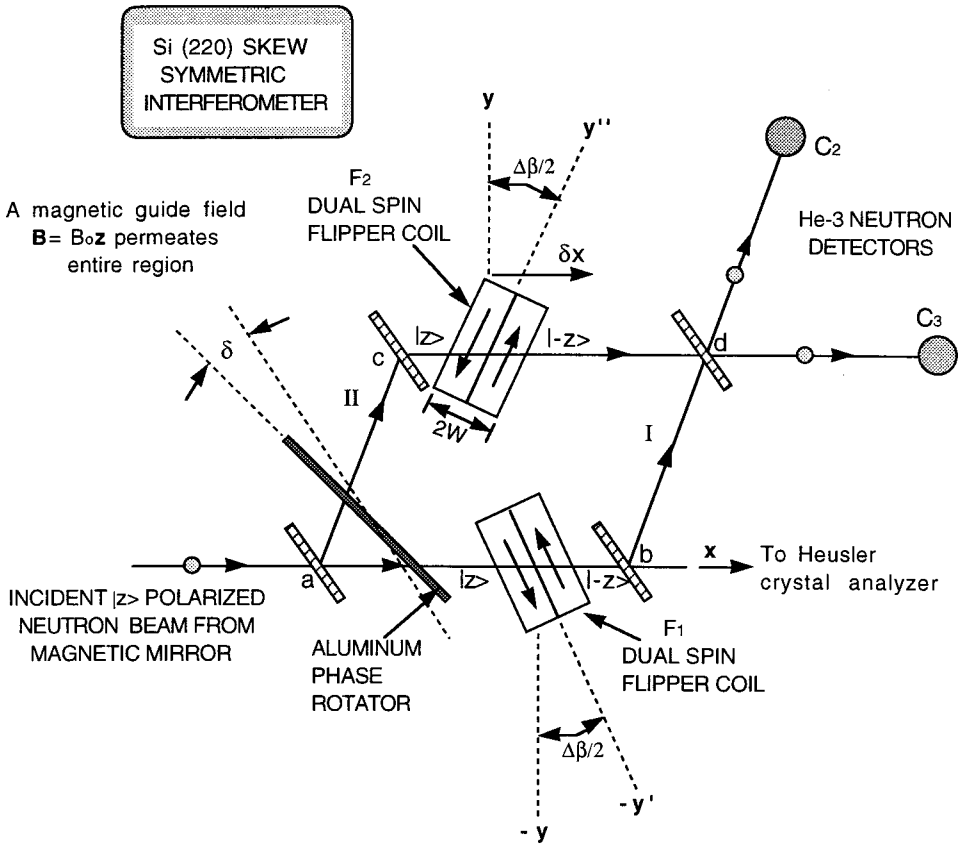

FIG. 1. Schematic diagram of the experiment to demarcate geometric and dynamical phases. A uniform vertical guide field $B_0\hat{\mathbf{z}}$ from a pair of Helmholtz coils is applied over the Si(220) skew symmetric interferometer. A relative rotation $\Delta\beta$ between the identical dual flippers F_1 and F_2 produces a pure geometric phase Φ_G, predicted to be equal to $\Delta\beta$, for the incident $|z\rangle$-polarized neutron beam; their relative translation δx results in a pure dynamical phase Φ_D, proportional to δx.

adiabatic evolution but a parallel transport [17] will effect an intrinsically nonadiabatic evolution. However, it is still possible to use a nonparallel transported state provided the dynamical phase can be made to disappear [17–19], as will now be described.

The basic idea of our experiment involves the interference of the neutron wave packets traversing the two separate paths in a Mach-Zehnder-type neutron interferometer after each wave packet has been individually spin flipped inside the interferometer. The clear demarcation of the geometric and dynamical phases occurs in the two physically distinct operations, a rotation and a translation, of the two spin flippers inside the interferometer. The initial proposal for the experiment was made by Wagh and Rakhecha [19], after their realization of the dependence of the spinor phase on the orientation of the precession axis [18], as is now explained.

The wave function of a spin-$\frac{1}{2}$ particle changes sign after a 2π precession [20,21]. This 4π spinor symmetry of the spin-$\frac{1}{2}$ particle, has been directly verified in both division-of-amplitude [22,23] and division-of-wave-front [24] neutron interferometry experiments. However, the spinor phase also depends on the orientation [18] of the precession axis.

In the present interferometric experiment with polarized neutrons, we perform a pair of π spin-flip operations, one in each arm of the interferometer, but with the two flipper axes enclosing an angle $\Delta\beta$. When the two flippers are identical, the Hamiltonian-dependent dynamical phases within the two flippers cancel each other. The dependence of the spinor phase on the orientation [18] of the precession axis manifests itself here as the Hamiltonian-independent geometric phase equal to minus half the solid angle $\Delta\Omega$ of the slice on the spin sphere, enclosed between the curves traced by the neutron spin within the two flippers. A relative translation between the two flippers, on the other hand, leaves the spin curves, and hence the geometric phase, unaltered, producing a pure dynamical phase due to the ambient guide field.

II. DESCRIPTION OF THE EXPERIMENT

Overview

The experiment is shown schematically in Fig. 1. A collimated, polarized, monochromatic neutron beam is incident on the first blade of a neutron interferometer. The monolithic, perfect-silicon-crystal neutron interferometer of skew-symmetric design sits in a region of uniform magnetic guide field $B_0\hat{\mathbf{z}}$. Bragg diffraction by the (220) planes at the first crystal plate coherently splits the neutron de Broglie wave packet. Each of the separated subbeams is again diffracted at the intermediate blades, and after passing through a spin flipper in the long arm of each path, overlap and interfere at the last blade. The recombined neutron wave packets are then detected by two ^{3}He proportional detectors, C_2 and C_3, beyond the interferometer. The interference appearing as a swapping of the detected neutron intensity in the recombined beams as a function of the phase difference between the

separate subbeams. The whole arrangement is akin to the Mach-Zehnder interferometer of classical optics. For a more detailed description of neutron interferometry, see Ref. [25].

A neutron in a magnetic field experiences Larmor precession. Here, a $|+z\rangle$ eigenstate gains dynamical phase as it precesses about the magnetic guide field, which also points in the z direction and leads up to the spin flipper. After being spin flipped, also incorporating a dynamical phase, the $|-z\rangle$ eigenstate also gains phase by precessing in the guide field, but of an opposite sense than the $|+z\rangle$ state before the spin flipper. This precession establishes some dynamical phase offset for the neutron's path. The experiment requires a spin flipper to change the polarization from $|+z\rangle$ to $|-z\rangle$. The simplest form of this flipper is a single horizontal field component $B_0\hat{\mathbf{y}}$ which requires the spin angular momentum $\mathbf{S}$ of the initial state $|+z\rangle$ to precess through an angle π on the spin sphere to the state $|-z\rangle$, as illustrated in Fig. 2(a). Rotating (without translating) a pair of such flippers inside an interferometer, one in each subbeam, to a relative orientation of angle $\Delta\beta$ between the two, results in the separate precession paths of $\mathbf{S}_{\mathrm{I}}$ and $\mathbf{S}_{\mathrm{II}}$ enclosing a solid angle $\Omega=-2\Delta\beta$ (an ''orange slice''), at the center of the spin sphere [26]. This manifests itself as a pure geometric phase shift

$$\Phi_G=-\Omega/2=\Delta\beta, \tag{2}$$

without altering the dynamical phase offset, i.e., without any dynamical phase shift contamination. This phase shift is independent of the Hamiltonian. In the experiment each flipper is actually a dual flipper producing successive π precessions about two mutually orthogonal axes, $\hat{\mathbf{q}}$ and $\hat{\mathbf{p}}$, say, directed 45° on either side of $\hat{\mathbf{z}}$ in the $\hat{\mathbf{y}}$-$\hat{\mathbf{z}}$ plane. This two-stage process precesses the $|+z\rangle$-polarized neutron state around the unit sphere of spin directions, to the state $|-z\rangle$. It is straightforward to show that their combined effect on the wave function of the neutron is equivalent to a precession around the y axis by an angle π. A second identical dual flipper oriented at $\Delta\beta$ to the first again results in a pure geometric phase, $\Phi_G=-\Omega/2=\Delta\beta$, as shown in Fig. 2(b).

A pure geometric phase can be achieved without any motion of the spin flipper at all. Reversing the current (and hence the direction of the magnetic field) in one dual flipper, is equivalent to affecting a 180° rotation of the precession axes without any physical motion [4,18], ensuring the original offset phases are unchanged. The dual flipper effects two successive π precessions about $\hat{\mathbf{q}}$ and $\hat{\mathbf{p}}$, respectively. Its operation,

$$e^{-i\sigma_p\pi/2}e^{-i\sigma_q\pi/2}=(-i\sigma_p)(-i\sigma_q)=-\sigma_p\sigma_q, \tag{3}$$

brings the $|+z\rangle$ state to $|-z\rangle$, where σ_q and σ_p represent two orthogonal components of the Pauli operator $\boldsymbol{\sigma}$ along $\hat{\mathbf{q}}$ and $\hat{\mathbf{p}}$, respectively. Reversing the current in the two coils of the dual flipper reverses the order of the two fields. The neutron is now subjected to a field first along $\hat{\mathbf{p}}$ followed by a field along $\hat{\mathbf{q}}$. This reversed flipper then operates as

$$e^{-i\sigma_q\pi/2}e^{-i\sigma_p\pi/2}=-\sigma_q\sigma_p=\sigma_p\sigma_q, \tag{4}$$

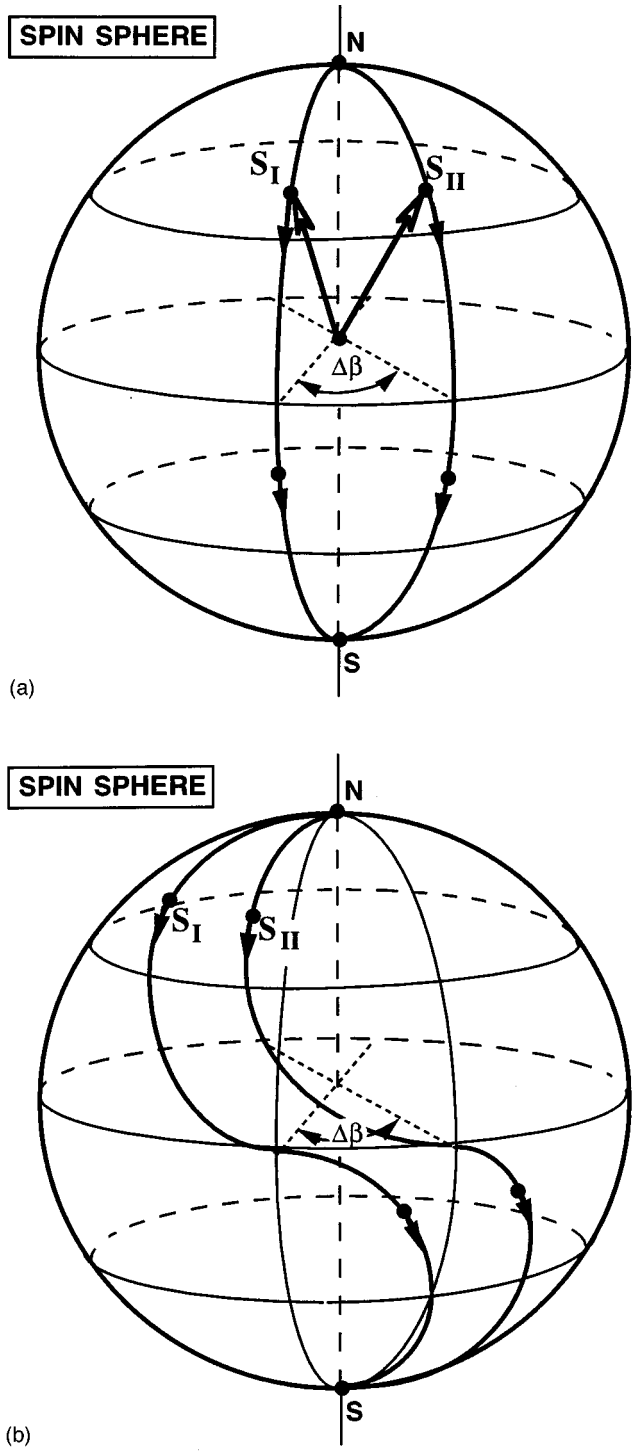

FIG. 2. Schematic of the path traced out by the neutron spin as it precesses around the spin sphere from spin-up, $|z\rangle$, to spin-down, $|-z\rangle$. The top figure, (a), shows the π precession of the spins $\mathbf{S}_{\mathrm{I}}$ and $\mathbf{S}_{\mathrm{II}}$ on the separate interferometer paths, each about a single horizontal field component oriented at an angle $\Delta\beta$ relative to the other. The lower figure, (b), shows the precession of the two spins $\mathbf{S}_{\mathrm{I}}$ and $\mathbf{S}_{\mathrm{II}}$ about the spin sphere under the action of the dual flipper. Here the two field components of the individual flipper, oriented at $+45°$ and $-45°$ to N-S on the same great circle ($\hat{\mathbf{p}}$ and $\hat{\mathbf{q}}$ in the text) result in successive π precessions. Again the second dual flipper is oriented at an angle $\Delta\beta$ to the first. In both cases, the geometric phase Φ_G is equal to half the solid angle between the two trajectories.

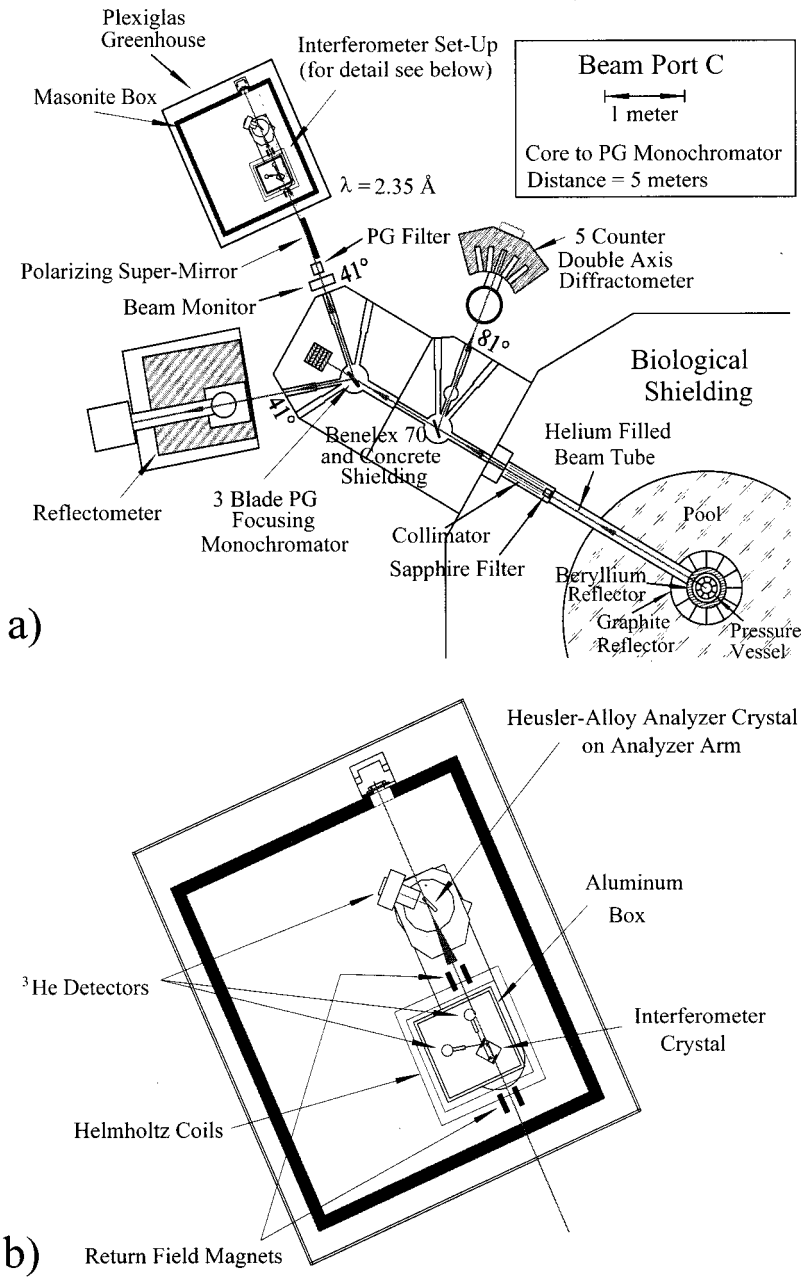

FIG. 3. Overall view of the *C*-port interferometer setup, including the reactor, beam port, shielding, polarizing supermirror, Helmholtz coils, interferometer, and Heusler alloy analyzing crystal. The inset shows a detail of the inside of the masonite box.

again taking the state $|+z\rangle$ to $|-z\rangle$, but with a change of sign compared to the previous situation, since σ_p and σ_q anticommutate, being orthogonal components of $\boldsymbol{\sigma}$. This sign change manifests itself as a π phase shift of the neutron interferogram [4,18]. Observation of this π phase shift would constitute, to our knowledge, the first direct verification of the anticommutativity of orthogonal components of the Pauli spin operator. We emphasize that a polarimetric experiment is incapable of detecting a current reversal in the flipper [27].

Finally, a linear translation δx of one of the spin flippers along the beam path results in the neutron spending more time in one spin orientation at the expense of the other, which changes the original Larmor precession phase distribution according to

$$\Delta\phi_L = 2\mu B_0 \delta x/\hbar v, \tag{5}$$

where μ and v are the neutron's magnetic moment and velocity, respectively. The translation is responsible for a purely dynamical phase [28]

$$\Phi_D = \Delta\phi_L . \tag{6}$$

Unlike the previous situation, the dynamical phase, being dependent on B_0 in the Hamiltonian, is generated, while leaving the spin trajectory on each path, and hence the offset geometric phase Φ_G, unaltered. A translation of the other flipper would generate an identical dynamical phase shift.

The purpose of this paper is to describe, in some detail, our neutron-interferometric observation of separate dynamical and geometric phases. Brief accounts of the results of this experiment have already been reported [29].

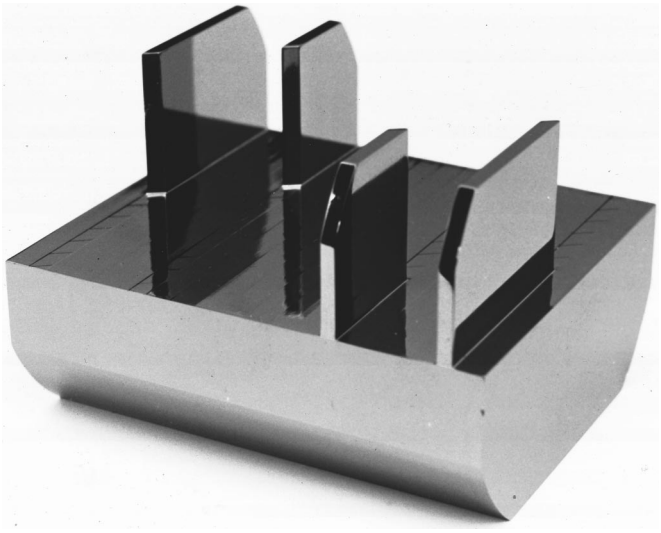

FIG. 4. Photograph of the single crystal Si skew-symmetric interferometer used in the experiment.

Experimental setup

The experiment was performed at the beam port *C* interferometer facility [30] at the University of Missouri Research Reactor (MURR) in a Bhabha Atomic Research Centre Vienna–Missouri collaboration. A schematic of the beam station is shown in Fig. 3. A thermal neutron beam from the reactor is incident on a vertically focusing three-crystal pyrolytic graphite (002) monochromator. The Bragg angle ($\theta_B = 20.5°$) is fixed by the exit tube, and yields a nominally monochromatic beam with $\lambda = 2.349$ Å ($\Delta\lambda/\lambda \approx 0.012$). A 5-cm-thick block of pyrolytic graphite filters the beam removing any second- ($\lambda/2$) and third-order ($\lambda/3$) neutrons. The neutrons from the monochromator were then polarized by reflection from a 50-cm-long, magnetic, Fe-Si multilayer supermirror ($\theta_c = 2\theta_{c\ \mathrm{Ni}} \cong 10$ mrad). The reflected, polarized 2-mm-wide beam passes through a 6-mm-high aperture at the entrance to an aluminum box and onto the first blade of the interferometer crystal. The interferometer, a single-silicon crystal with four blades, in skew-symmetric alignment (see Fig. 4), has been described in several experiments [30]. The interferometer (resting in a cradle) and two ^{3}He proportional detectors are housed in the aluminum box (with clear Plexiglas lid), providing for an isothermal enclosure. This box is rigidly mounted to an 850-kg black granite slab which supports a $1.0 \times 1.2 \times 1.8$ m^3 Benelex-70 masonite box (again with Plexiglas lid) enclosing the Al box. The granite slab rests on four Firestone pneumatic vibration isolators mounted on steel posts embedded in sand enclosures. Hanging below the slab is a large Al plate supporting 710 kg of lead bricks, which are used to lower the center of gravity of the optical table. An all-encompassing Plexiglas greenhouse provides additional environmental isolation against temperature gradients and microphonics due to air currents.

A uniform vertical ($+\hat{\mathbf{z}}$) magnetic guide field is provided over the entire experimental region by a pair of water-cooled Cu-wire Helmholtz coils wound on horizontal 52-cm square aluminum formers with a vertical separation of 7 cm (centered in height about the beam path through the crystal). These are placed around the Al box containing the interferometer crystal. To compensate for the return field (along $-\hat{\mathbf{z}}$) of the Helmholtz coils, two pairs of small permanent magnets were placed either side of the beam as it entered and exited the Al box. This maintained a uniform guide field

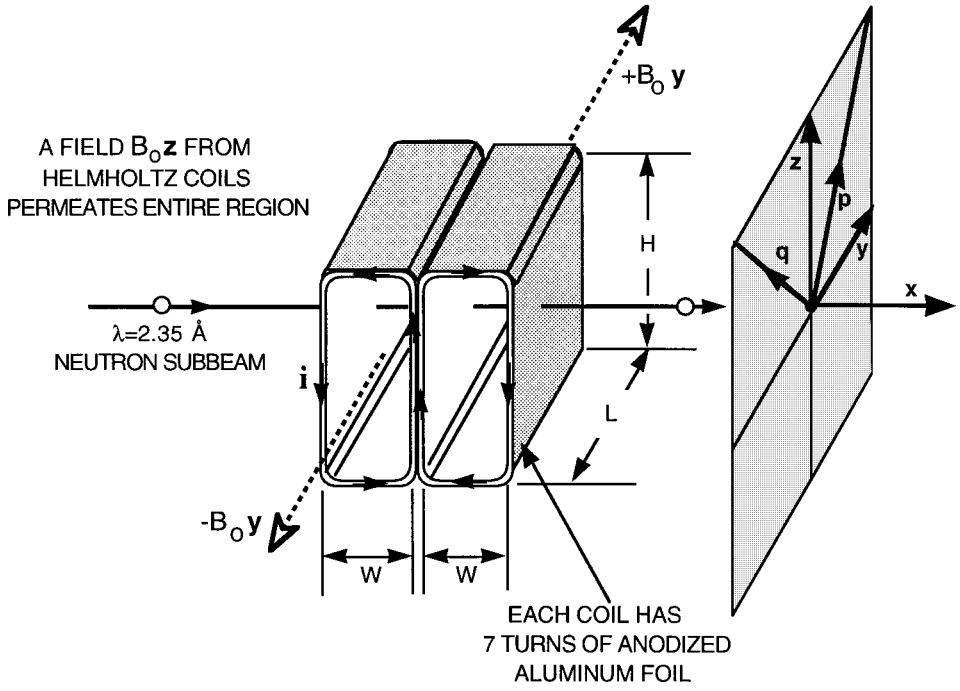

FIG. 5. Cross-sectional view of the dual flipper showing the neutron trajectory through the anodized aluminum foil windings of the coils. The horizontal magnetic field, $B_0\hat{\mathbf{y}}$ of the individual coils when added to the vertical environment field, $B_0\hat{\mathbf{z}}$, of the Helmholtz coils results in a field directed in the $\hat{\mathbf{q}}$ direction for the first coil and in the $\hat{\mathbf{p}}$ direction for the second directed at $-\pi/4$ and $\pi/4$ to $\hat{\mathbf{z}}$, respectively. It is these directions about which the neutron precesses.

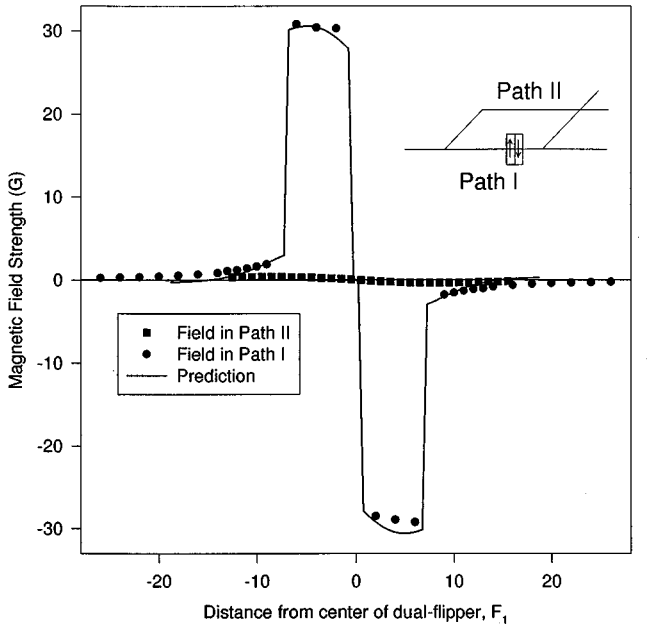

FIG. 6. A map of the transverse field component $B_0\hat{\mathbf{y}}$ of dual flipper F_1 along the neutron trajectory through the interferometer. The circles represent the measured transverse field on the path of the spin flipper. A theoretical prediction is indicated by the line. The squares are the measured field values extending onto the opposite interferometer path. The centers of the two beams have a measured separation of 22 mm, so there is very little field overlap between the two dual flippers.

along the $\hat{\mathbf{z}}$ direction over the entire neutron path. The basic layout of the experiment described to this point is identical to that used in a neutron interferometric measurement of multiphoton exchange amplitudes [31] that had just been completed.

Essential to the operation of the experiment were the spin flippers. As already mentioned, spin flipping was achieved in a two-stage process, illustrated in Fig. 5. First, the $|+z\rangle$ polarized neutron state enters a region of magnetic field, $\sqrt{2}B_0\hat{\mathbf{q}}$ (the vector sum of the guide field $B_0\hat{\mathbf{z}}$ and the flipper coil field $-B_0\hat{\mathbf{y}}$), oriented at $-45°$ in the $\hat{\mathbf{y}}$-$\hat{\mathbf{z}}$ plane perpendicular to the neutrons direction of motion $\hat{\mathbf{x}}$. The magnitude of the field in this region is set so that while traversing the coil the neutron spin precesses by an azimuthal angle π, in a plane perpendicular to $\hat{\mathbf{p}}$, the precession axis, becoming oriented in the $-\hat{y}$ direction, half way on its journey to $|-z\rangle$. The $|-y\rangle$-polarized neutron then enters a similar region of magnetic field directed along $\hat{\mathbf{p}}$, orthogonal to $\hat{\mathbf{q}}$, at $+45°$ in the $\hat{\mathbf{y}}$-$\hat{\mathbf{z}}$ plane. The neutron again precesses through an azimuthal angle π about $\hat{\mathbf{p}}$ to the $|-z\rangle$ state. In measuring the geometric phase, the spin flippers are rotated in a plane perpendicular to $\hat{\mathbf{z}}$, so that $\hat{\mathbf{p}}$ and $\hat{\mathbf{q}}$ now lie in the $\hat{\mathbf{y}}'$-$\hat{\mathbf{z}}$ plane, as shown in Fig. 1.

To produce the two precessions responsible for the spin flipping, each spin flipper consisted of two back-to-back rectangular coils shown in Fig. 5. The two rectangular coils, 25 mm long×15 mm high×7 mm wide, were placed across the neutron path with the long axis horizontal, so that the neutron beam had a 7-mm path through each of the coils (W in Fig. 5). The two coils were connected in series, but were wound with opposite orientation producing horizontal magnetic fields of the same magnitude but opposite sense. The transverse field component of one flipper as measured along each beam path is shown in Fig. 6. Each coil is wound around two pegs defining their top and bottom which are attached to a TeCu-145 heat-sink block. An individual coil, with self-supporting sides, consisted of seven turns of 25-mm-wide, 90-μm-thick anodized Al foil. Low-temperature Al to Cu brazing provided excellent electrical contact between the coil and the Cu leads. To reduce thermal gradients in the vicinity of the crystal, a thin Cu sheet enclosed the ends of the coils. This sheet was clamped between two Cu plates attached either side of the heat-sink block. The heat-sink blocks were water cooled by a closed-loop water circuit, with the temperature of the coils and block monitored and maintained to 0.01 °C accuracy. Under operating conditions (operating current of 7 A), the water circuit removed about 4 W of heat per dual flipper. Each spin flipper was suspended in the long parallel paths of skew-symmetric interferometer, and rigidly attached to a precision translation-rotation mechanism (built in the Missouri Physics Machine Shop). High precision was needed in positioning the spin flippers, as the nuclear phase shift when rotating the flippers, due to the change in effective length of the neutron path through the various materials of the flipper coils and housing, was orders of magnitude larger than the expected geometrical phase. The experimental geometry allowed sufficient space to translate each spin flipper about 10 mm along the beam path and rotate each one to $\pm 22°$. A photograph of the water-cooled spin flippers attached to the precision translation-rotation mechanism is shown in Fig. 7.

The spin-flipping efficiency of the flippers could be measured using an Heusler alloy analyzer crystal placed in the undeflected beam beyond the aluminum box. Optimization of the spin flipper, F_1, in the undeflected arm was achieved by adjusting the resultant magnetic field $\mathbf{B}_0$ produced by the vertical Helmholtz coil component and the horizontal flipper component (each with magnitude ≈ 30 G), in a procedure that will be explained later.

Experimental strategy

In the neutron interferometer the neutron-counting rates in the recombined beams, detected by the ^{3}He counters C_2 and C_3 are given by

$$N_2 = N_1(a_2 - b_2\cos\Delta\phi) \tag{7}$$

and

$$N_3 = N_1(a_3 + b_3\cos\Delta\phi), \tag{8}$$

where $\Delta\phi$ is the phase shift along path II relative to path I, and N_1 is the counting rate in the monitor counter C_1. The constants a_2, a_3, b_2, and b_3 such that $a_2/a_3 \approx 2.5$ and $b_2 \approx b_3$, characterize the interferometer. It is found that $N_2 + N_3$ is independent of $\Delta\phi$, i.e., as $\Delta\phi$ is varied the neutrons are swapped back and forth between C_2 and C_3 (as expected by particle conservation), showing that b_2 and b_3 are equal.

A common practice is to introduce a spin-independent phase shift α by inserting a thin aluminum (1.05 mm thick) plate across both beams and rotating it through an angle δ.

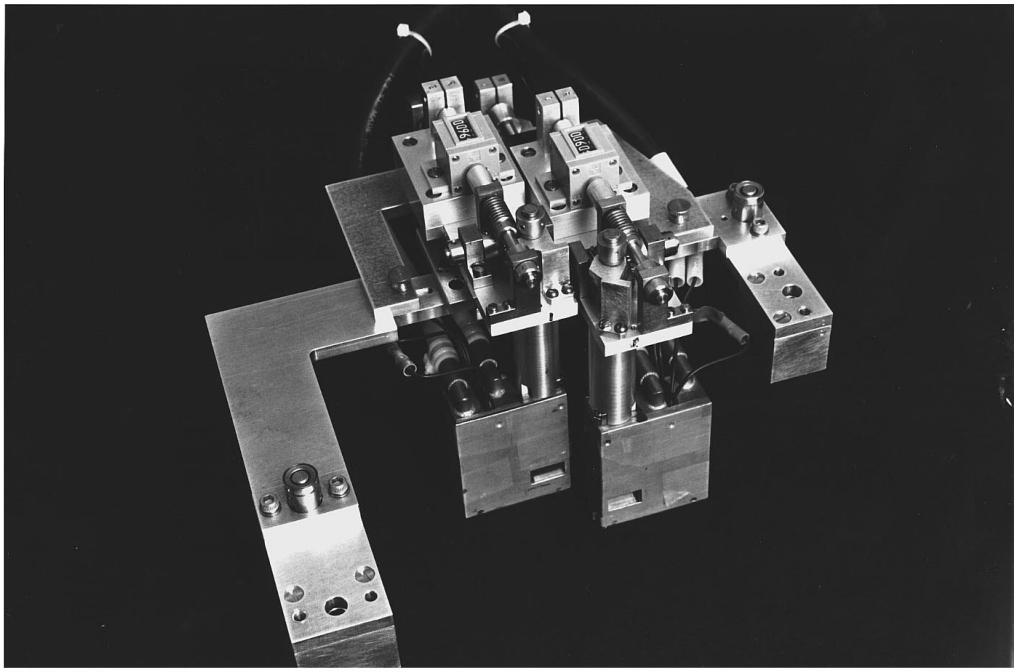

(a)

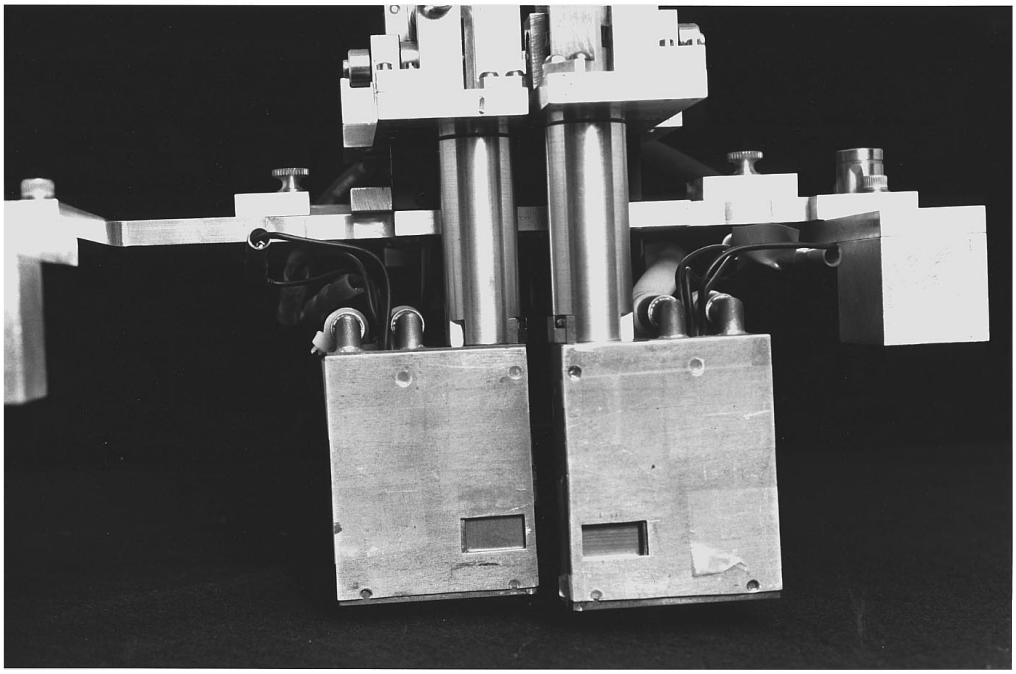

(b)

FIG. 7. Photograph of the precision translation-rotation mechanism (top) and the water-cooled heat-sink blocks (hanging below) containing spin-flipping coils. The blocks are then lowered into the long parallel paths of the neutron interferometer so that the neutron subbeams pass through the Cu windows and Al coils in the lower corner of each block.

Figure 8 shows an example of just such an interferogram with a fringe contrast of 64%. The total phase may then be written as

$$\Delta\phi = \alpha + \alpha_0 + \Delta\Phi_{\text{tot}},$$

$$= \alpha + \gamma, \tag{9}$$

where α_0 is the spin-independent offset phase of the interferometer, and $\Delta\Phi_{\text{tot}}$ is the total spin-dependent phase in the presence of the magnetic field of the Helmholtz coils and spin flippers. The term $\gamma = \alpha_0 + \Delta\Phi_{\text{tot}}$ represents the offset phase determined from fitting the interferogram with

$$N_3 = N_1[a_3 + b_3\cos(\alpha + \gamma)] \tag{10}$$

as a function of α. By switching the spin flippers on and off

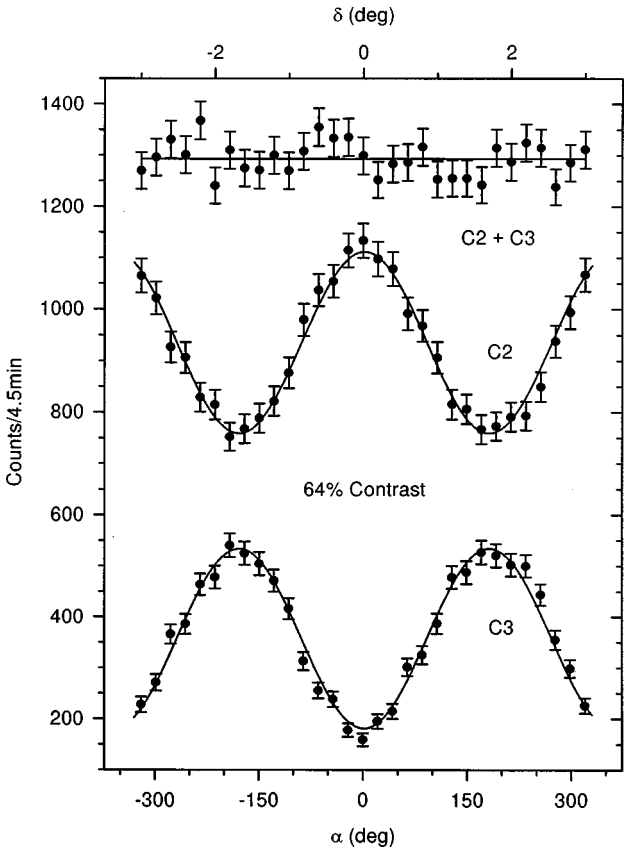

FIG. 8. Plot of the counts achieved in the ^{3}He detectors, $C2$ and $C3$, for the empty interferometer, as a function of the spin-independent phase α, achieved by rotating the Al phase flag across both subbeams by an angle δ.

and interleaving data collection, two interferograms are recorded simultaneously. An example of the ''flipper-off'' and ''flipper-on'' interferograms, with contrasts of 32% and 28%, respectively, are shown in Fig. 9. The difference in contrast is mainly due to the change in the neutron's kinetic energy by the amount $2\mu B_0$ when being rotated from the spin-up state to the spin-down state, which leads to a slight change in the reflectivity of the Bragg reflections at the subsequent crystal slabs [32]. For the flipper-on case the offset phase is

$$\gamma_{\rm on} = \alpha_0 + \Delta\Phi_{\rm tot}^{\rm on}, \tag{11}$$

while for the flipper-off case

$$\gamma_{\rm off} = \alpha_0 + \Delta\Phi_{\rm tot}^{\rm off}. \tag{12}$$

Consequently, the difference

$$\Delta\gamma = \gamma_{\rm on} - \gamma_{\rm off} = \Delta\Phi_{\rm tot}^{\rm on} - \Delta\Phi_{\rm tot}^{\rm off} \tag{13}$$

corresponds to the total spin-dependent phase shift between the flipper-on and flipper-off interferograms. This procedure eliminates the effect of time-dependent drifts in the spin-independent phase α_0 within the interferometer due to various environmental effects. This was found to be less than 5° per day. The spin-dependent magnetic phase shifts were found to be very stable.

The experiment was performed in three parts. In the first instance, as already mentioned, a pure geometric phase shift is achieved by a relative rotation $\Delta\beta$ of the spin flippers, one by an angle $+\Delta\beta/2$ and the other by $-\Delta\beta/2$. Interference is then observed for a range of angles $\Delta\beta/2$ from $-20°$ to $+20°$. In the second case, a geometric phase of π can be affected without any physical motion of the flipper. With the spin flippers normal to the beam path, the current to each in turn is reversed by the mere flick of a switch. This corresponds to rotating the spin flipper through 180°. A flipper-on–flipper-off pair of interferograms was made for each permutation of current directions. Finally, for a measurement of a purely dynamical phase shift, the spin flippers remain perpendicular to the beam ($\Delta\beta/2=0$), and first one and then the other is translated in 2-mm steps for $\approx$10 mm along the respective subbeam neutron paths. Interleaved flipper-on–flipper-off interferograms are again made at each of these positions.

III. EXPERIMENTAL RESULTS

The following experimental procedure was used for each part of the experiment: At each experimental setting a phase rotator scan is made with the flippers sequentially switched on and off every 60 000 monitor counts (5 s) for a total of 5×10^6 monitor counts per point (7.5 min). A single interferogram pair took 8 h to perform. The on-off period is much shorter than the thermal time constants of the dual-flipper heat sinks. By recording two interferograms simultaneously, a difference measurement could be made that eliminated the spin-independent nuclear phase shifts due to the heating of the flipper materials and thermal gradients inside the interferometer. An example of the flipper-on and flipper-off interferogram pair is shown in Fig. 9. The phase difference between these two is the spin-dependent phase shift of interest. The difference phases $\Delta\gamma=\gamma_{\rm on}-\gamma_{\rm off}$ for a series of runs are then plotted after requiring that all the flipper-off interferograms overlap at the same offset value. The offset value used as the constant reference corresponded to the experimental conditions $\Delta\beta/2=0$, F_1 at $x_1=39$ mm and F_2 at $x_2=39$ mm from the first blade of the interferometer.

To measure the geometric phase, the spin flippers were individually rotated in opposite directions, to $+\Delta\beta/2$ and $-\Delta\beta/2$, through the angular range $\Delta\beta/2=-20°$ to $+20°$ in 5° steps. This was done so that the nuclear phase shift acquired in passing through the windings of the coils canceled nearly identically. Rotation of the dual flipper increased the path length by $W/\cos(\Delta\beta/2)$, necessitating the appropriate reduction in field to maintain precise spin flipping. For example at 20°, B_0 should be reduced by 4%. However, in the experiment we kept B_0 fixed, and later corrected the phase shift for excess spin flip. This correction ranged between 0° and 8°. Figure 10 displays examples of the flipper-on geometric phase interferograms which have all been shifted relative to the concurrently recorded flipper-off interferograms overlap. The phase advance of the interferogram is clearly seen. The lines are fits based on Eq. (10). A summary of the entire geometric phase data set is shown in Fig. 11, plotted against $\Delta\beta$, the angle between the two flippers. The actual on-off phase difference is shown on one ordinate, and the geometric phase shift (relative to the reference condition) on

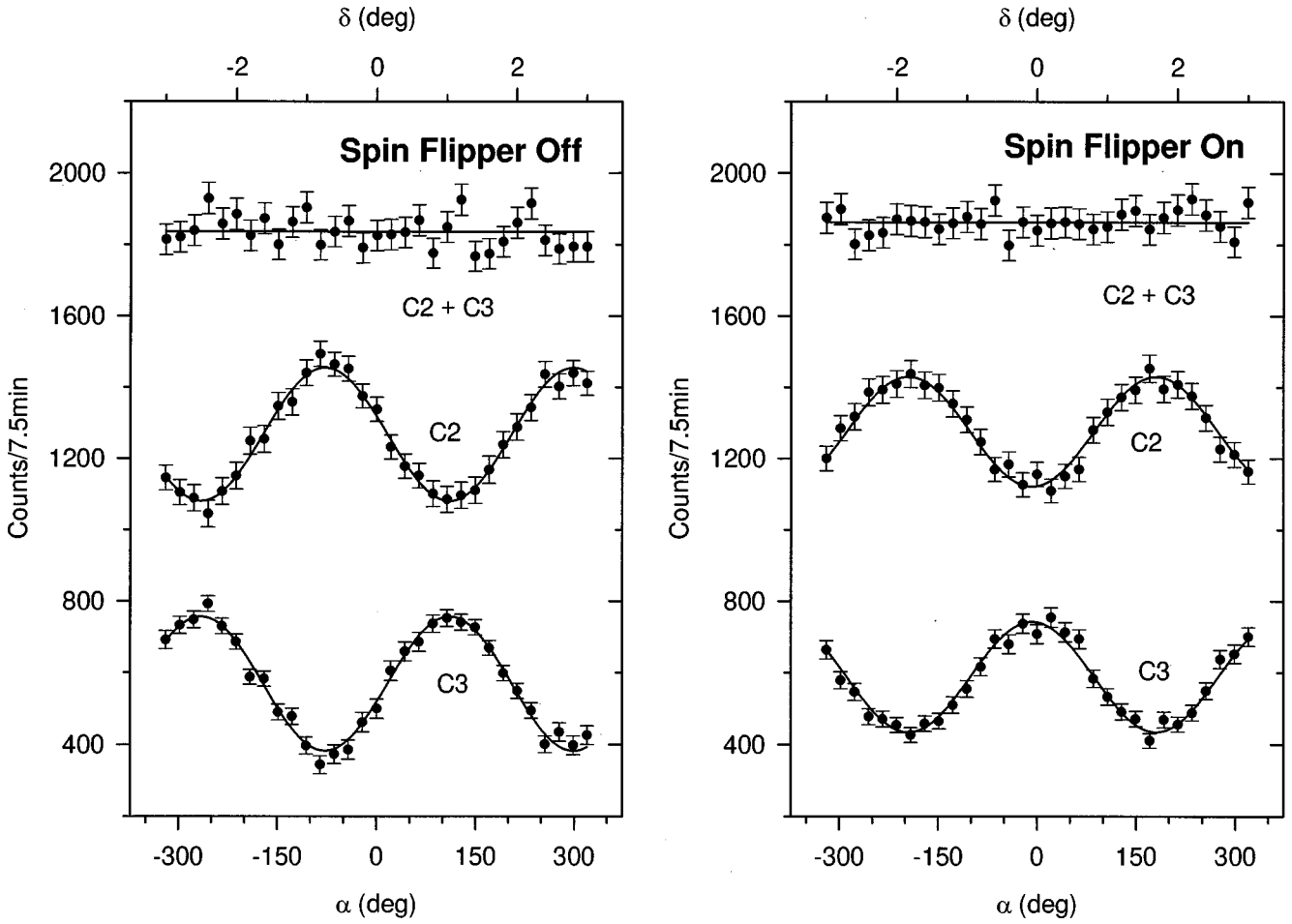

FIG. 9. Plots of the nuclear neutron interferograms achieved by rotating the Al phase flag with the spin-flipping coils in place in the interferometer for the two cases of spin flipper off and on, i.e., when a current is not applied to the coils and when one is. The phase difference between these two interferograms is $\Delta\gamma$, used to measure the dynamical and geometric phases.

the other. The line represents a theoretical fit, and will be explained below.

With the spin flippers oriented perpendicular to the respective subbeams, another measure of the geometric phase could be affected without mechanical rotation, simply by reversing the current applied to each dual flipper in turn. Such a current reversal reverses the magnetic field direction of the coil, and is equivalent to rotating the individual flipper by 180°. A plot of the (shifted relative to the flipper-off interferograms) flipper-on interferograms for the four possible combinations of the flipper fields is shown in Fig. 12. It is seen that each current reversal shifts the interferogram by π. The lines are fits again based on Eq. (10), and the values of the fitted phases γ are shown in the corner of each plot. The average phase shift from the top plot to the bottom is $182.3° \pm 2.4°$, and confirms the anticommutativity of σ_p and σ_q. This phase shift is of purely geometric origin, and constitutes the first direct verification of Pauli anticommutation.

To achieve a measure of the dynamical phase, the flippers (oriented perpendicular to the beam) are translated in 2-mm steps on path I and then on path II, with interferograms made at each step. A plot of the dynamical phase advance of a set of shifted flipper-on interferograms for each path is shown in Fig. 13. Summaries of these phase shifts are shown in Figs. 14 and 15. The line represents a theoretical fit, as will now be explained.

Data analysis

In an ideal experiment, the neutron beam incident on the interferometer would be 100% polarized in the $|+z\rangle$ state, and the action of the spin flipper would have this state flipped perfectly to the $|-z\rangle$ state. Unfortunately, in this experiment, neither the supermirror nor either dual flipper were 100% efficient. This meant that the final interference included neutrons initially distributed in the two spin states, some of which were then flipped by the action of the spin flipper and some that were not. This added greatly to the complexity of the data analysis.

First, consider the distribution of neutron intensities. Defining P as the polarization of the beam incident from the polarizing supermirror, then

$$P = \frac{I_{\uparrow}^{0} - I_{\downarrow}^{0}}{I_{\uparrow}^{0} + I_{\downarrow}^{0}}, \tag{14}$$

where $I_{\uparrow}^{0}$ and $I_{\downarrow}^{0}$ are the intensities of spin-up and spin-down neutrons after the mirror, and the total incident intensity is $I_0 = I_{\uparrow}^{0} + I_{\downarrow}^{0}$. The values of $I_{\uparrow}^{0}$ and $I_{\downarrow}^{0}$ are found from the maxima (perfect spin flipping) and minima (no spin flipping), respectively, of the data in Fig. 16(a), i.e., the neutron intensity measured by the Heusler polarization analyzing

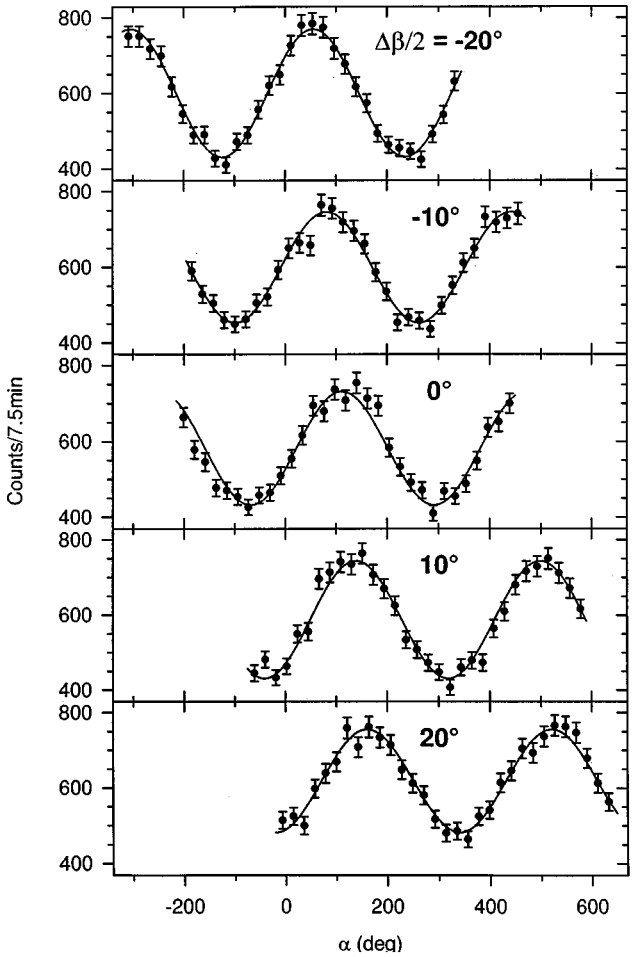

FIG. 10. A series of the nuclear interferograms showing the advance of the geometric interference phase over the range of relative angular separations $\Delta\beta$ of the two dual flippers. The angular separation is achieved by physically rotating the coil in path I to an angle $+\Delta\beta/2$, and one in path II to $-\Delta\beta/2$.

crystal as a function of the field strength of the spin flipper F_1. These intensities give $P=0.85$.

Similarly, the combined efficiency of the two coils of a flipper, f, may be defined by

$$f=\frac{I_{\uparrow}^{f}-I_{\downarrow}^{f}}{I_{\uparrow}^{f}+I_{\downarrow}^{f}}, \tag{15}$$

where $I_{\uparrow}^{f}$ and $I_{\downarrow}^{f}$ are the intensities of spin-up and spin-down neutrons detected. The value of f, from the actual measured values of the spin flipper and Helmholtz fields, differed from 1 by at most 1% in the dynamical data due to nonuniformity in the Helmholtz field as the flipper was translated (see Fig. 17). In the geometric data, f varied by as much as 8% at the extreme setting, $\Delta\beta/2=20°$. This was a consequence of the dual flipper's magnetic field not being scaled as the path length increased through the flipper by $W/\cos(\Delta\beta/2)$ as the flipper was rotated. The resultant number of spin-down neutrons detected is given by

$$\begin{aligned} I_{\downarrow}&=\left(\frac{f+1}{2}\right)I_{\uparrow}^{0}+\left(\frac{1-f}{2}\right)I_{\downarrow}^{0} \\ &=\left(\frac{f+1}{2}\right)\left(\frac{P+1}{2}\right)I_0+\left(\frac{1-f}{2}\right)\left(\frac{1-P}{2}\right)I_0, \end{aligned} \tag{16}$$

In this expression the first term represents those spin-up neutrons incident on the spin flipper that are flipped, and the second those incident spin down neutrons that are not flipped. Accounting for the efficiency of the two parts of the individual dual flipper by f_1 and f_2, this expression becomes

$$\begin{aligned} I_{\downarrow}&=\left[\left(\frac{f_1+1}{2}\right)\left(\frac{f_2+1}{2}\right)\right]^{1/2}\left(\frac{P+1}{2}\right)I_0 \\ &+\left[\left(\frac{1-f_1}{2}\right)\left(\frac{1-f_2}{2}\right)\right]^{1/2}\left(\frac{1-P}{2}\right)I_0. \end{aligned} \tag{17}$$

The same is true for the spin-up neutrons detected, where

$$\begin{aligned} I_{\uparrow}&=\left[\left(\frac{1-f_1}{2}\right)\left(\frac{1-f_2}{2}\right)\right]^{1/2}\left(\frac{P+1}{2}\right)I_0 \\ &+\left[\left(\frac{f_1+1}{2}\right)\left(\frac{f_2+1}{2}\right)\right]^{1/2}\left(\frac{1-P}{2}\right)I_0. \end{aligned} \tag{18}$$

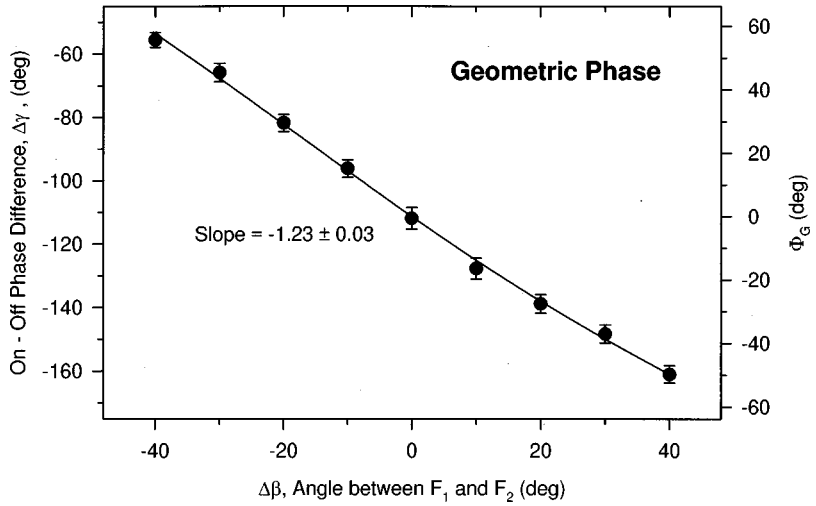

FIG. 11. Plot of the on-off phase difference for the entire geometric phase data set, as a function of the angle between the spin flippers achieved by physically rotating the two spin flippers. The right abscissa shows the equivalent value of the geometric phase Φ_G. The line represents a theoretical fit, as explained in the text.

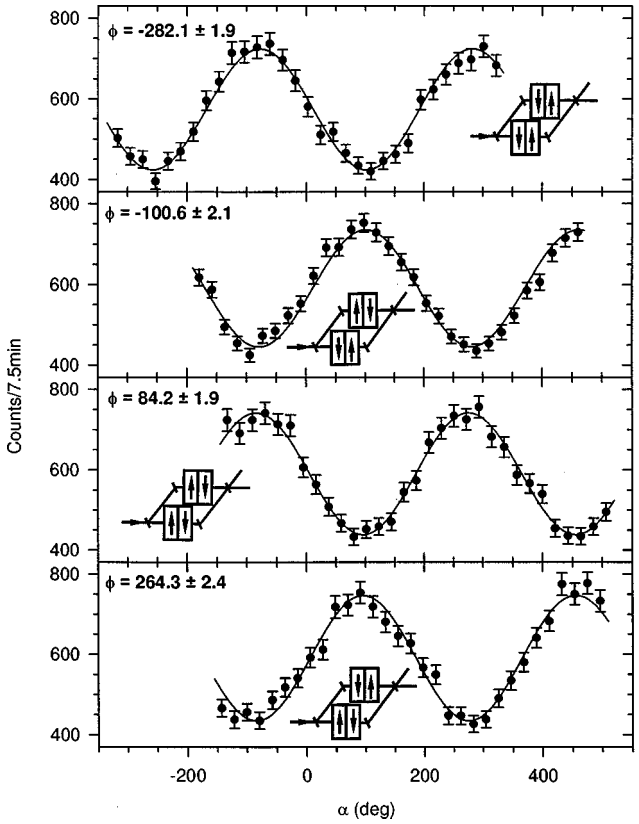

FIG. 12. Series of interferograms showing the $182.3° \pm 2.4°$ phase shift as the current is reversed to each of the dual flippers in turn. This π phase shift accurately verifies Pauli anticommutation to within about 1.3%.

The experimental optimization of the current applied to spin flipper F_1 (in the direct beam), and the current in the Helmholtz coils to flip an incident spin-up neutron to the spin-down state is shown in Figs. 16(a) and 16(c), respectively. The maxima of these plots establishes the condition $f_1 = 1$, perfect spin flipping. The currents appropriate for this condition were $I_H = 1.549$ A and $I_{F_1} = 7.357$ A. We were unable to perform the same optimization for F_2, in the twice-deflected subbeam on path II, as the neutron intensity was too low to give a meaningful measurement. Consequently, it was assumed that the two dual flippers were identical, a fair assumption given the uniformity of materials, structure, and production.

In the experiment, the currents used were $I_H = 1.55$ A and $I_{F_1} = 7.3$ A. These currents generated the magnetic field responsible for flipping the neutron spin. A current of 7.3 A generated a measured magnetic-field strength of 29.9 G in the upstream coil and 28.4 G in the downstream coil of the dual flipper F_1. A plot of the measured (points) and theoretical (line) field strengths due to the coils in spin flipper F_1 as a function of position along the beam path is shown in Fig. 6. In F_2, the measured fields were 28.5 G in the upstream coil and 29.6 G in the downstream coil. At the reference positions of the dual flippers, the vertical field strength of the pair of Helmholtz coils and return field magnets was 30.2 and 29.6 G for the upstream and downstream coils of F_1, respectively. The corresponding values for F_2 were 30.8 and 29.9 G. A field map along the neutron trajectory through the interferometer is shown in Fig. 17.

The experiment measures the difference in the spin-dependent offset phase between the flipper-on and flipper-off interferograms, as determined by a least-squares fit at each setting, namely,

$$\Delta\gamma = \Delta\Phi_{\text{tot}}^{\text{on}} - \Delta\Phi_{\text{tot}}^{\text{off}}. \tag{19}$$

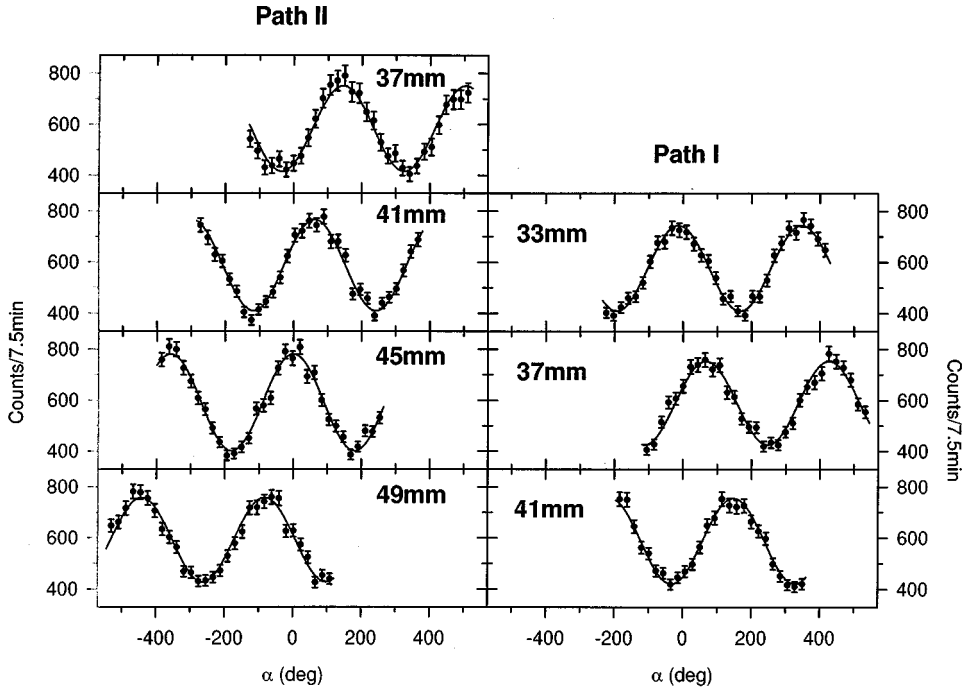

FIG. 13. A series of nuclear interferograms showing the advance of the dynamical interference phase over the range of relative translations (from the first interferometer blade) of the dual flippers in the two paths of the interferometer.

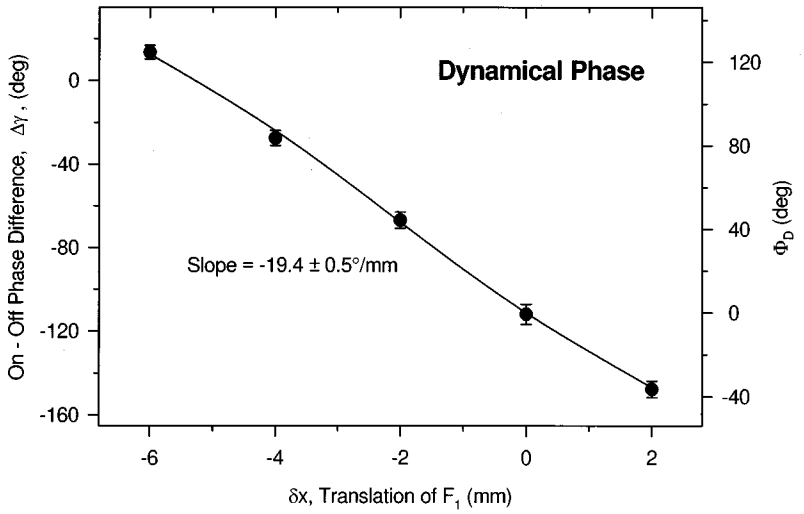

FIG. 14. Plot of the on-off phase difference as a function of translation of F_1 along path I, measured relative to the reference position (39 mm) from the first blade of the interferometer. The right axis shows the equivalent value of the dynamical phase. The line represents a theoretical fit, as explained in the text.

To first consider the effect of imperfect initial polarization, set $f=1$ (perfect spin flipping). For spin-up incident neutrons, the interferogram detected in C_3 has the general form

$$N_{3\uparrow}=\left(\frac{P+1}{2}\right)N_1\{a_3+b_3\cos(\alpha+\alpha_0+\Delta\Phi)\}, \qquad (20)$$

where $(\alpha+\alpha_0)$ and $\Delta\Phi$ are the total spin-independent and total spin-dependent phases respectively. Similarly, for spin-down neutrons,

$$N_{3\downarrow}=\left(\frac{1-P}{2}\right)N_1\{a_3+b_3\cos(\alpha+\alpha_0-\Delta\Phi)\}. \qquad (21)$$

The total interferogram is then the sum due to the two spin components,

$$N_3=N_{3\uparrow}+N_{3\downarrow}=N_1\{a_3+b_3[P\ \sin(\alpha+\alpha_0)\sin\Delta\Phi + \cos(\alpha+\alpha_0)\cos\Delta\Phi]\}. \qquad (22)$$

This interferogram is of the form

$$N_3=N_1\{a_3+b_3'\cos(\alpha+\alpha_0+\Delta\Phi_{\rm tot})\} = N_1\{a_3+b_3'[\cos(\alpha+\alpha_0)\cos\Delta\Phi_{\rm tot} - \sin(\alpha+\alpha_0)\sin\Delta\Phi_{\rm tot}]\}, \qquad (23)$$

where $\Delta\Phi_{\rm tot}$ is the observed spin-dependent phase of interest, that is, the spin-dependent offset phase in the flipper-on and flipper-off interferograms. Hence, the measured phase $\Delta\Phi_{\rm tot}$ is dependent upon the actual spin-dependent phase of interest $\Delta\Phi$ by the relation

$$\tan\Delta\Phi_{\rm tot}=P\ \tan\Delta\Phi. \qquad (24)$$

The observed amplitude and actual amplitude are related by

$$b_3'^2=b_3^2[P^2\sin^2\Delta\Phi+\cos^2\Delta\Phi]. \qquad (25)$$

Including the effects of imperfect spin flipping complicates these expressions considerably. We now summarize the calculation of the combined corrections of imperfect incident

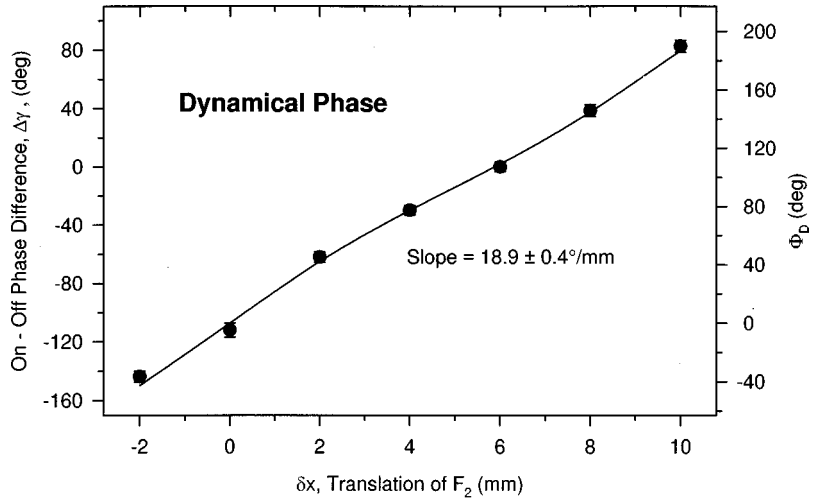

FIG. 15. Plot of the on-off phase difference as a function of translation of F_2 along path II, measured relative to the reference position (39 mm) from the first blade of the interferometer. The right axis shows the equivalent value of the dynamical phase. The line represents a theoretical fit, as explained in the text.

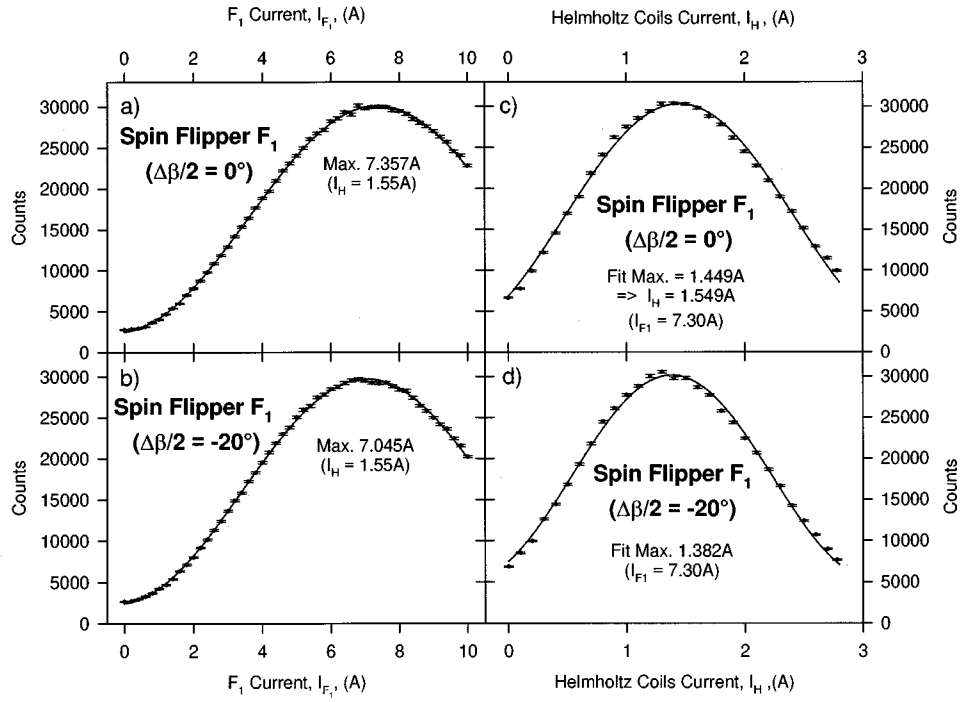

FIG. 16. Plot of the intensity of spin-down component of the beam incident on the Heusler analyzer crystal as a function of current applied (proportional to the horizontal magnetic-field component $B_0\hat{\mathbf{y}}'$) to the dual flipper F_1, when oriented (a) normal to the neutron beam, and (b) with the flipper oriented at 20° from normal incidence. The current corresponding to the maximum in (b), should, by geometry, equal $I_{\mathrm{MAX}\,0^\circ}/\cos(20^\circ)$. Both of these measurements were made for a Helmholtz coil current of 1.55 A ($B_0\hat{\mathbf{z}}\approx 30$ G). A fit to (a) was used to determine the $(2\,\mu W/\hbar v)$ factor used to scale the action of the dual flipper F_1, as described in the text. Plot of the analyzed intensity of spin-down neutrons as a function of current applied (proportional to the vertical field component $B_0\hat{\mathbf{z}}$) to the Helmholtz coils, (c) when F_1 is oriented normal to the incident neutron beam, and (d) with the flipper oriented at 20° from normal incidence. Again, the current corresponding to the maximum in (d), should, by geometry, equal $I_{\mathrm{MAX}\,0^\circ}/\cos(20^\circ)$. Both of these measurements were made for a dual-flipper current of 7.3 A ($B_0\hat{\mathbf{y}}'\approx 30$ G). The solid lines to the data represent fits, as explained in the text.

beam polarization and flipping efficiencies of the flippers. The detailed derivations are given in the Appendix.

To obtain the geometric phase from the measured interferogram phases, we must separately consider the fraction $(1+P)/2$ of spin-up incident neutrons and the fraction $(1-P)/2$ of spin-down incident neutrons. When the dual flippers are switched on, the total spin-dependent phase shift of the interferogram as a function of $\Delta\beta$, namely, $[\Delta\Phi^{\mathrm{on}}_{\mathrm{tot}}(\Delta\beta)]$, for spin-up incident neutrons and spin-down incident neutrons is given by

$$\tan[\Delta\Phi^{\mathrm{on}}_{\mathrm{tot}}(\Delta\beta)]=P\,\frac{\sqrt{(1-f_{\mathrm{I}})(1-f_{\mathrm{II}})}\sin\Delta\Phi^{\mathrm{on}}_{\uparrow\uparrow}(\Delta\beta)+\sqrt{(1+f_{\mathrm{I}})(1+f_{\mathrm{II}})}\sin\Delta\Phi^{\mathrm{on}}_{\uparrow\downarrow}(\Delta\beta)}{\sqrt{(1-f_{\mathrm{I}})(1-f_{\mathrm{II}})}\cos\Delta\Phi^{\mathrm{on}}_{\uparrow\uparrow}(\Delta\beta)+\sqrt{(1+f_{\mathrm{I}})(1+f_{\mathrm{II}})}\cos\Delta\Phi^{\mathrm{on}}_{\uparrow\downarrow}(\Delta\beta)}. \tag{26}$$

(This expression is derived in the Appendix.) In this expression, $\Delta\Phi^{\mathrm{on}}_{\uparrow\uparrow}(\Delta\beta)$ $[=-\Delta\Phi^{\mathrm{on}}_{\downarrow\downarrow}(\Delta\beta)]$ and $\Delta\Phi^{\mathrm{on}}_{\uparrow\downarrow}(\Delta\beta)$ $[=-\Delta\Phi^{\mathrm{on}}_{\downarrow\uparrow}(\Delta\beta)]$ are the spin-dependent phases for incident spin-up neutrons remaining unflipped and those being flipped, respectively, by the action of the dual flippers, given by Eqs. (A22) and (A23) in the Appendix. The flipping efficiencies of the dual flippers are denoted f_{I} and f_{II} for paths I and II, respectively. The spin-dependent phase differences for path II minus path I for incident spin-up neutrons which are not spin flipped is $\Delta\Phi_{\uparrow\uparrow}$; for those spin flipped it is $\Delta\Phi_{\uparrow\downarrow}$. Similarly, the phase differences for incident spin-down neutrons are $\Delta\Phi_{\downarrow\downarrow}$ and $\Delta\Phi_{\downarrow\uparrow}$.

In the case where there is no current applied to the spin flippers, the expression is much simpler. This situation corresponds to the neutron precessing about the vertical guide field while traversing the interferometer, so that the total spin-dependent phase is

$$\tan\Delta\Phi^{\mathrm{off}}_{\mathrm{tot}}(\Delta\beta)=P\,\tan(\Delta\phi^0_{A+B}+\Delta\phi^0_{C+D}). \tag{27}$$

[see Eq. (A31) in the Appendix], where $\Delta\phi^0_{A+B}$ is the dynamical phase accumulated on path II due to the precession

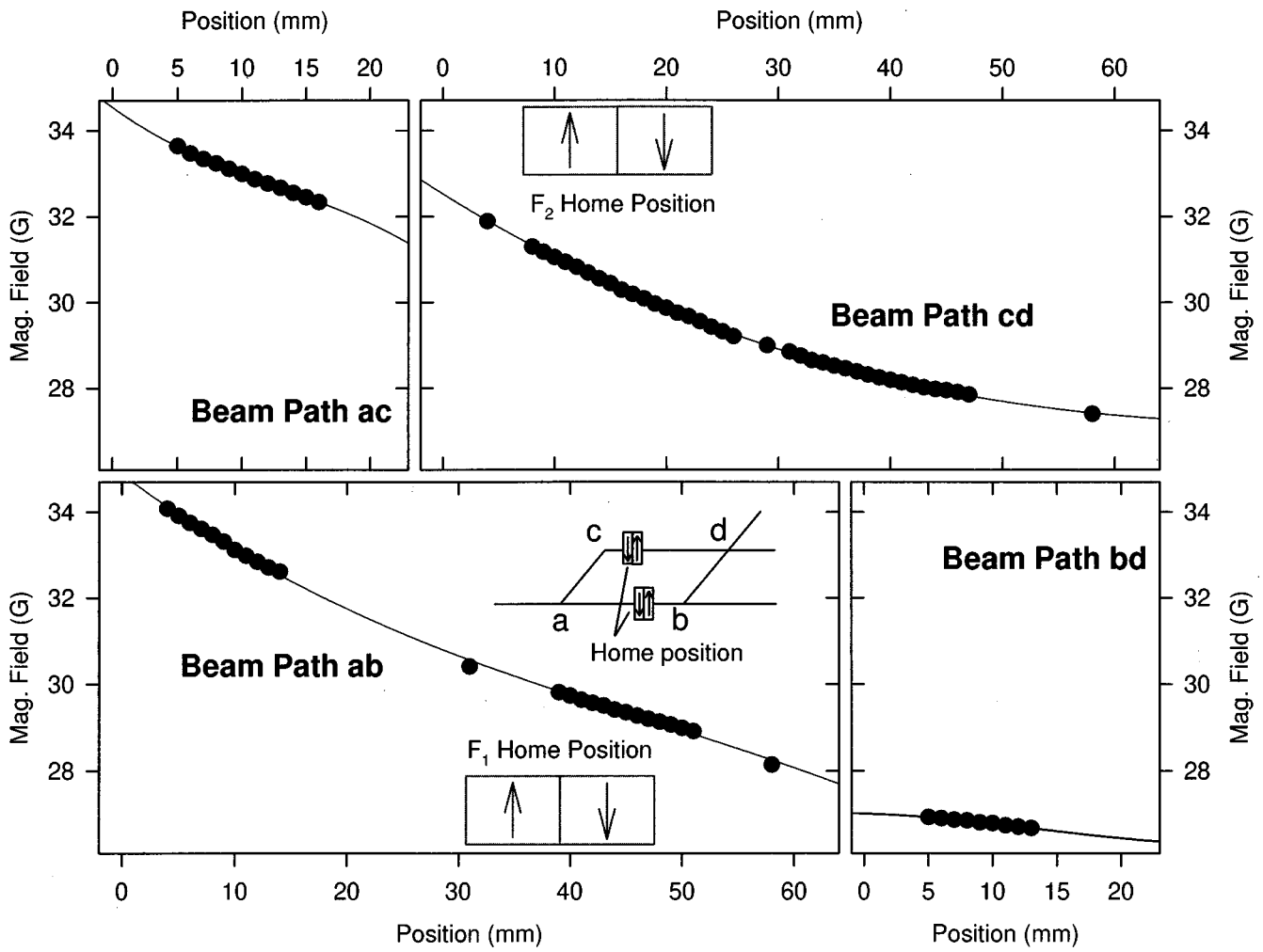

FIG. 17. Map of the vertical field component $B\hat{\mathbf{z}}$ due to the Helmholtz coils for all positions inside the interferometer. These field values are used in the calculation of the spin-flipping efficiency of the two dual flippers.

about the vertical Helmholtz coil field, with the flippers turned off, from the first blade of the interferometer to the middle of the dual flipper minus the same phase accumulated on path I. Similarly, $\Delta\phi^0_{C+D}$ is the dynamical phase accumulated on path II due to the precession about the vertical Helmholtz coil field, with the flippers turned off, from the middle of the dual flipper to the last blade of the interferometer minus the same phase accumulated on path I. In the experiment the data actually measured is $\Delta\gamma(\Delta\beta)$, the measured phase difference between the on and off interferograms as a function of $\Delta\beta$, given by Eq. (19).

As explained in the Appendix, the constant terms in the phase determination were experimentally determined using the optimization curve of Fig. 16(a), which was fit as a function of the applied current. Having scaled the action of the spin flipper, by these experimentally measured constants, a fit was made to the geometric phase data of Fig. 11. A simple linear regression to the data, has a slope of -1.36 ± 0.04. After correction for incident polarization and nonperfect spin-flipping using Eqs. (26) and (27), the slope becomes -1.23 ± 0.03. The line in Fig. 11 represents this fit. According to Eq. (2), $\Phi_G=\Delta\beta$; then, theoretically, the slope of the data should equal -1. However, in the fitting procedure, any dynamical phase contamination appearing in the results will be accounted for in the slope (see the Appendix). The flipper translation-rotation mechanism did not allow for an accurate positioning of the rotation axis of each flipper over the center line of the subbeam. Consequently, rotation of an off-center flipper would be accompanied by a displacement δx along the beam and therefore a dynamical phase component. A combined off-centeredness for the two flippers of 0.8 mm is sufficient to generate a Φ_D to account for the observed deviation from the expected slope of the data. Note that the geometric phase measurements achieved by reversing the current to the flippers are free from any dynamical phase component.

In the dynamical phase measurement, the spin flipper is set perpendicular to the incident beam ($\Delta\beta=0$), and the spin flipper is translated along each beam. As the spin-flipper is translated inside the interferometer, it moves through a region of varying magnetic-field strength $B_0\hat{\mathbf{z}}$, as shown in Fig. 17. Here $\Delta\gamma$ is fit as a function of δx (as explained in the Appendix) for the two cases of a translation along paths I and II. Results of the fits to the two cases are shown as lines in Figs. 14 and 15. The slopes of these two data sets are $-19.4°\pm0.5°/\text{mm}$ and $18.9°\pm0.4°/\text{mm}$, respectively.

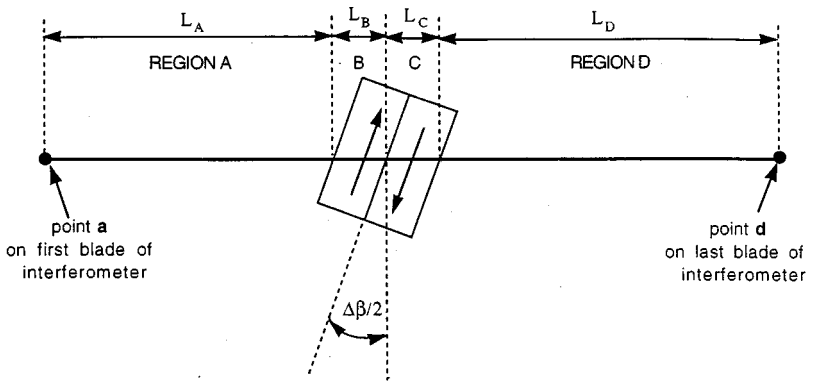

FIG. 18. Figure showing the four sections of the neutron subbeam path through the interferometer used in the determination of the spin-dependent geometric and dynamical phases.

These slopes correspond to field strengths of 31.0 ± 0.7 and 30.3 ± 0.6 G, respectively, as calculated from Eq. (5), which agree to within a few percent with the measured averages (as seen in Fig. 17) over these regions of 29.9 ± 0.1 and 30.3 ± 0.1 G.

IV. CONCLUSION

We have performed a polarized neutron interferometry experiment where, by means of dc spin flippers in both beams, geometric and dynamical phase shifts could be individually controlled and observed. This experiment affects a clean separation of geometric and dynamical phases, a consequence of the spinor phase dependence on the orientation of the precession axis. The dynamical phase shift is proportional to the difference in path length that the neutron passed in a spin-up state and then in a spin-down state in the two arms of the interferometer. A pure dynamical phase is produced by a relative translation of the two dual flippers. The geometric phase has a true geometric expression in the experimental layout, as it corresponds to the angle between the magnetic fields of the spin flippers. A reversal of the current applied to a flipper, equivalent to changing the angle between the two flippers by 180°, generates a pure geometric phase of π, and its observation confirms the anticommutativity of orthogonal components of the Pauli spin operators.

ACKNOWLEDGMENTS

The success of this work depended greatly upon the skilled workmanship of Clifford Holmes and his staff at the Physics Machine Shop at Missouri. This work was carried out under the Austrian Funds (FWF) Project No. P9266-PHY, the NSF–Physics Division, Grant No. 9603559, and a UM Research Board Grant No. RB-94-003. One of us (A.G.W.) wishes to acknowledge support for two months from the Austrian Funds, and for one month from the University of Missouri–Columbia during the experiment. B.E.A. would like to acknowledge support from an Australian Research Council grant during the writing of this paper.

APPENDIX: CORRECTIONS DUE TO THE COMBINED EFFECTS OF NONIDEAL BEAM POLARIZATION AND FLIPPING EFFICIENCY

In this appendix we give a derivation of the formulas we used to correct the measured interferogram phases for the combined effects of imperfect polarization and spin flipping to obtain the geometric and dynamical phases. On each subbeam I and II, the neutron path through the interferometer is broken into four sections, as shown in Fig. 18. The first, called A, from the first blade of the interferometer to the front edge of the spin flipper, corresponds to a length L_A; the second, B, the first coil of the dual flipper, corresponds to a length L_B; the third, C, the second coil, to a length L_C; and the fourth, D, from the back edge of the spin flipper to the last blade of the interferometer, to a length L_D. It is possible to write the effect on the spinor neutron wave function traversing each of these regions in terms of a transfer matrix M. For regions A and D, in the presence of the vertical Helmholtz field only, such a transfer matrix is diagonal and has the form

$$M = \begin{bmatrix} e^{i\phi} & 0 \\ 0 & e^{-i\phi} \end{bmatrix}, \tag{A1}$$

where ϕ is the dynamical phase accumulated due to precession in the vertical field. In the spin-flipping regions of B and C, with both horizontal and vertical fields, the transfer matrix is

$$M = \begin{bmatrix} \cos\phi + i \sin\phi \cos\xi & -\sin\phi \sin\xi e^{-i\Delta\beta/2} \\ \sin\phi \sin\xi e^{i\Delta\beta/2} & \cos\phi - i \sin\phi \cos\xi \end{bmatrix}. \tag{A2}$$

The wave function for a spin-up incident neutron after traversing the four sections on either path I or II of the interferometer under the action of the spatially dependent fields is given by the product of the four transfer matrices, i.e., $M_D M_C M_B M_A$. Writing out the matrix multiplications, we have

$$\psi = e^{ik_0x}e^{i\alpha}\left\{\begin{array}{l}\left[\begin{array}{c}\cos\phi_B\cos\phi_C-\sin\phi_B\cos\xi_B\sin\phi_C\cos\xi_C-\sin\phi_B\sin\xi_B\sin\phi_C\sin\xi_C\\ +i(\sin\phi_B\cos\xi_B\cos\phi_C+\sin\phi_C\cos\xi_C\cos\phi_B)\end{array}\right]e^{i(\phi_A+\phi_D)}|\uparrow\rangle \\ +\left[\begin{array}{c}(-\cos\phi_B\sin\phi_C\sin\xi_C-\cos\phi_C\sin\phi_B\sin\xi_B)\\ +i(-\sin\phi_B\cos\xi_B\sin\phi_C\sin\xi_C+\sin\phi_B\sin\xi_B\sin\phi_C\cos\xi_C)\end{array}\right]e^{-i\Delta\beta/2}e^{i(\phi_A-\phi_D)}|\downarrow\rangle\end{array}\right\}, \tag{A3}$$

where

$$\phi_A=\frac{\mu B_Z L_A}{\hbar v},\quad \phi_B=\frac{\mu B L_B}{\hbar v},$$

$$\phi_C=\frac{\mu B L_c}{\hbar v},\quad \phi_D=\frac{\mu B_Z L_D}{\hbar v}. \tag{A4}$$

The neutron's magnetic moment and velocity are μ and v, respectively. The strength of the magnetic field in the spin-flipper region is given by

$$B=\sqrt{B_z^2+B_{y'}^2}, \tag{A5}$$

the vector sum of the vertical Helmholtz field B_Z and the transverse horizontal flipper coil field $B_{y'}$. The precession axis $\hat{\mathbf{p}}$ or $\hat{\mathbf{q}}$ of a single spin-flipper coil is at an angle ξ to $\hat{\mathbf{z}}$ such that $\cos\xi=B_Z/B$ and $\sin\xi=B_{y'}/B$. Finally we will define $\Delta\phi_A$ to be the difference phase shift due to Larmor precession about the guide field in region A on the two subbeam paths I and II, so that $\Delta\phi_A=\phi_A^{\rm II}-\phi_A^{\rm I}$. Similarly $\Delta\phi_B$, $\Delta\phi_C$, and $\Delta\phi_D$ are the difference phase shifts in each of regions B, C, and D respectively, $\Delta\phi_B$ and $\Delta\phi_C$ being a measure of the phase associated with the spin-flipping regions, and with $\Delta\phi_D=\phi_D^{\rm II}-\phi_D^{\rm I}$ the difference in precession phase accumulated in regions D of paths I and II.

Equation (A3) may then be written as

$$\psi^{\rm II}=e^{ik_0x_{\rm II}}e^{i\alpha_{\rm II}}\left[\left(\frac{1-f_{\rm II}}{2}\right)^{1/2}e^{i\chi_{\uparrow{\rm II}}}e^{i(\phi_A+\phi_D)_{\rm II}}|\uparrow\rangle -\left(\frac{f_{\rm II}+1}{2}\right)^{1/2}e^{i\chi_{\downarrow{\rm II}}}e^{i(\phi_A-\phi_D)_{\rm II}}e^{-i\Delta\beta_{\rm II}}|\downarrow\rangle\right] \tag{A6}$$

for path II, and

$$\psi^{\rm I}=e^{ik_0x_{\rm I}}e^{i\alpha_{\rm I}}\left[\left(\frac{1-f_{\rm I}}{2}\right)^{1/2}e^{i\chi_{\uparrow{\rm I}}}e^{i(\phi_A+\phi_D)_{\rm I}}|\uparrow\rangle -\left(\frac{f_{\rm I}+1}{2}\right)^{1/2}e^{i\chi_{\downarrow{\rm I}}}e^{i(\phi_A-\phi_D)_{\rm I}}e^{-i\Delta\beta_{\rm I}}|\downarrow\rangle\right] \tag{A7}$$

for path I. Here $f_{\rm I}$ is the flipping efficiency defined above, and can be written as

$$\begin{aligned}f_{\rm I}&=\left[\frac{I_\uparrow^f-I_\downarrow^f}{I_\uparrow^f+I_\downarrow^f}\right]_{\rm I}\\ &=[\beta_B\beta_C\sin2\phi_B\sin2\phi_C\\ &\quad-\beta_B\alpha_B\beta_C\alpha_C(1-\cos2\phi_B)(1-\cos2\phi_C)\\ &\quad-(\alpha_B^2+\beta_B^2\cos2\phi_B)(\alpha_C^2+\beta_C^2\cos2\phi_C)]_{\rm I},\end{aligned} \tag{A8}$$

where $\alpha_B\equiv\cos\xi_B$ and $\beta_B\equiv\sin\xi_B$ for the first coil, and $\alpha_C\equiv\cos\xi_C$ and $\beta_C\equiv\sin\xi_C$ for the second coil of the dual flipper, and the bracket $[\ ]_{\rm I}$ means that the quantities inside the bracket are evaluated along subbeam I. An equivalent expression applies to subbeam II.

The two wave functions in Eqs. (A6) and (A7) produce an interference pattern as a function of the nuclear phase α, where α represents the difference in nuclear phase between path II and I achieved by rotating the Al phase plate, and is given by $\alpha=\alpha_{\rm II}-\alpha_{\rm I}$. In these expressions k_0x refers to the standard spin-independent phase accumulated along each path, which is responsible for the interferometer offset phase $\alpha_0=k_0x_{\rm II}-k_0x_{\rm I}$. Traversing the dual spin flipper in path I, the neutron accumulates a phase $\chi_{\rm I}\uparrow$ if it is not flipped, and $\chi_{\rm I\downarrow}$ if it is spin flipped. Similar expressions apply to path II. The desired geometric phase appears in the term $\Delta\beta=\Delta\beta_{\rm II}-\Delta\beta_{\rm I}$.

In either path, spin flipping only occurs when a current is applied to the spin flipper. In this case (for incident spin-up neutrons),

$$\begin{aligned}e^{i\chi_\uparrow^{\rm on}}&=(\cos\phi_B+i\alpha_B\sin\phi_B)(\cos\phi_C+i\alpha_C\sin\phi_C)\\ &\quad-\beta_B\beta_C\sin\phi_B\sin\phi_C\end{aligned} \tag{A9}$$

and

$$\begin{aligned}e^{i\chi_\downarrow^{\rm on}}&=-\beta_C\sin\phi_C(\cos\phi_B+i\alpha_B\sin\phi_B)\\ &\quad-\beta_B\sin\phi_B(\cos\phi_C-i\alpha_C\sin\phi_C)\end{aligned} \tag{A10}$$

are the terms in the wave function for the non-spin-flipped and spin-flipped neutrons, respectively, after traversing regions B and C, the spin flippers. Therefore

$$\tan\chi_\uparrow^{\rm on}(\Delta\beta)=\frac{\alpha_C\sin\phi_C(\Delta\beta)\cos\phi_B(\Delta\beta)+\alpha_B\cos\phi_C(\Delta\beta)\sin\phi_B(\Delta\beta)}{\cos\phi_C(\Delta\beta)\cos\phi_B(\Delta\beta)-\alpha_C\alpha_B\sin\phi_C(\Delta\beta)\sin\phi_B(\Delta\beta)-\beta_C\beta_B\sin\phi_C(\Delta\beta)\sin\phi_B(\Delta\beta)} \tag{A11}$$

and

$$\tan\chi_\downarrow^{\rm on}(\Delta\beta)=\frac{(\alpha_B\beta_C-\alpha_C\beta_B)\sin\phi_C(\Delta\beta)\sin\phi_B(\Delta\beta)}{\beta_B\cos\phi_C(\Delta\beta)\sin\phi_B(\Delta\beta)+\beta_C\sin\phi_C(\Delta\beta)\cos\phi_B(\Delta\beta)}. \tag{A12}$$

The terms that make up this expression (which we will evaluate later) are based on the measured magnetic-field strengths, so the phase shifts $\chi_{\uparrow}^{\rm on}(\Delta\beta)$ and $\chi_{\downarrow}^{\rm on}(\Delta\beta)$ can be determined.

The general intensity distribution detected in C_3 for incident spin-up neutrons is

$$N_{3\uparrow\uparrow}=\left[\left(\frac{1-f_{\rm I}}{2}\right)\left(\frac{1-f_{\rm II}}{2}\right)\right]^{1/2}\left(\frac{P+1}{2}\right)\times N_1\{a_3+b_3\cos(\alpha+\alpha_0+\Delta\Phi_{\uparrow\uparrow}^{\rm on})\} \quad \text{(A13)}$$

for the nonflipped neutrons and

$$N_{3\uparrow\downarrow}=\left[\left(\frac{1+f_{\rm I}}{2}\right)\left(\frac{1+f_{\rm II}}{2}\right)\right]^{1/2}\left(\frac{P+1}{2}\right)\times N_1\{a_3+b_3\cos(\alpha+\alpha_0+\Delta\Phi_{\uparrow\downarrow}^{\rm on})\} \quad \text{(A14)}$$

for flipped neutrons. The total spin-dependent phase shifts are given by

$$\Delta\Phi_{\uparrow\uparrow}^{\rm on}(\Delta\beta)=\Delta\phi_A(\Delta\beta)+\Delta\phi_D(\Delta\beta)+\Delta\chi_{\uparrow}^{\rm on}(\Delta\beta) \quad \text{(A15)}$$

and

$$\Delta\Phi_{\uparrow\downarrow}^{\rm on}(\Delta\beta)=\Delta\phi_A(\Delta\beta)-\Delta\phi_D(\Delta\beta)-\Delta\beta+\Delta\chi_{\downarrow}^{\rm on}(\Delta\beta), \quad \text{(A16)}$$

where $\Delta\chi_{\uparrow}^{\rm on}=\Delta\chi_{\rm II\uparrow}^{\rm on}-\Delta\chi_{\rm II\uparrow}^{\rm on}$ and $\Delta\chi_{\downarrow}^{\rm on}=\Delta\chi_{\rm II\downarrow}^{\rm on}-\Delta\chi_{\rm I\downarrow}^{\rm on}$. The resultant intensity for spin-up incident neutrons is then

$$\begin{aligned}N_{3\rm up}&=N_{3\uparrow\uparrow}+N_{3\uparrow\downarrow}\\&=\left(\frac{P+1}{2}\right)N_1\left\{\begin{array}{l}\left[\left(\frac{1-f_{\rm I}}{2}\right)\left(\frac{1-f_{\rm II}}{2}\right)\right]^{1/2}\{a_3+b_3[\cos(\alpha+\alpha_0)\cos(\Delta\Phi_{\uparrow\uparrow}^{\rm on})-\sin(\alpha+\alpha_0)\sin(\Delta\Phi_{\uparrow\uparrow}^{\rm on})]\}\\+\left[\left(\frac{f_{\rm I}+1}{2}\right)\left(\frac{f_{\rm II}+1}{2}\right)\right]^{1/2}\{a_3+b_3[\cos(\alpha+\alpha_0)\cos(\Delta\Phi_{\uparrow\downarrow}^{\rm on})-\sin(\alpha+\alpha_0)\sin(\Delta\Phi_{\uparrow\downarrow}^{\rm on})]\}\end{array}\right\}.\end{aligned} \quad \text{(A17)}$$

This may be written as

$$\begin{aligned}N_{3\rm up}&=\left(\frac{P+1}{2}\right)N_1\{a_{3\rm up}+b_{3\rm up}\cos(\alpha+\alpha_0+\Delta\Phi_{\rm up}^{\rm on})\}\\&=\left(\frac{P+1}{2}\right)N_1\{a_{3\rm up}+b_{3\rm up}[\cos(\alpha+\alpha_0)\cos\Delta\Phi_{\rm up}^{\rm on}-\sin(\alpha+\alpha_0)\sin\Delta\Phi_{\rm up}^{\rm on}]\},\end{aligned} \quad \text{(A18)}$$

where $\Delta\Phi_{\rm up}^{\rm on}$ is the observed total spin-dependent phase for spin-up incident neutrons, such that

$$\tan\Delta\Phi_{\rm up}^{\rm on}=\frac{\sqrt{(1-f_{\rm I})(1-f_{\rm II})}\sin\Delta\Phi_{\uparrow\uparrow}^{\rm on}+\sqrt{(1+f_{\rm I})(1+f_{\rm II})}\sin\Delta\Phi_{\uparrow\downarrow}^{\rm on}}{\sqrt{(1-f_{\rm I})(1-f_{\rm II})}\cos\Delta\Phi_{\uparrow\uparrow}^{\rm on}+\sqrt{(1+f_{\rm I})(1+f_{\rm II})}\cos\Delta\Phi_{\uparrow\downarrow}^{\rm on}}. \quad \text{(A19)}$$

All of the above equations apply to the fraction $(1+P)/2$ of the incident beam that is spin-up.

We must now add to these results the intensities for the fraction $(1-P)/2$ of the incident beam that is spin-down. By symmetry, it is straightforward to do this. We have

$$N_{3\downarrow\downarrow}=\left[\left(\frac{1-f_{\rm I}}{2}\right)\left(\frac{1-f_{\rm II}}{2}\right)\right]^{1/2}\left(\frac{1-P}{2}\right)N_1\{a_3+b_3\cos(\alpha+\alpha_0+\Delta\Phi_{\downarrow\downarrow}^{\rm on})\} \quad \text{(A20)}$$

for the nonflipped neutrons and

$$N_{3\downarrow\uparrow}=\left[\left(\frac{f_{\rm I}+1}{2}\right)\left(\frac{f_{\rm II}+1}{2}\right)\right]^{1/2}\left(\frac{1-P}{2}\right)N_1\{a_3+b_3\cos(\alpha+\alpha_0+\Delta\Phi_{\downarrow\uparrow}^{\rm on})\} \quad \text{(A21)}$$

for flipped neutrons. By symmetry, the spin-dependent phase shifts are given by

$$\Delta\Phi_{\downarrow\downarrow}^{\rm on}=-\Delta\phi_A-\Delta\Phi_D-\Delta\chi_{\downarrow}^{\rm on}=-\Delta\Phi_{\uparrow\uparrow}^{\rm on} \quad \text{(A22)}$$

and

$$\Delta\Phi_{\downarrow\uparrow}^{\rm on}=-\Delta\phi_A+\Delta\phi_D+\Delta\beta-\Delta\chi_{\downarrow}^{\rm on}=-\Delta\Phi_{\uparrow\downarrow}^{\rm on}, \quad \text{(A23)}$$

the negative of the spin-up case. The resultant intensity is then

$$N_{3\text{down}}=N_{3\downarrow\downarrow}+N_{3\downarrow\uparrow}$$
$$=\left(\frac{1-P}{2}\right)N_1\left\{\begin{array}{l}\left[\left(\frac{1-f_{\rm I}}{2}\right)\left(\frac{1-f_{\rm II}}{2}\right)\right]^{1/2}\{a_3+b_3[\cos(\alpha+\alpha_0)\cos(\Delta\Phi^{\rm on}_{\uparrow\uparrow})+\sin(\alpha+\alpha_0)\sin(\Delta\Phi^{\rm on}_{\uparrow\uparrow})]\}\\ +\left[\left(\frac{f_{\rm I}+1}{2}\right)\left(\frac{f_{\rm II}+1}{2}\right)\right]^{1/2}\{a_3+b_3[\cos(\alpha+\alpha_0)\cos(\Delta\Phi^{\rm on}_{\uparrow\downarrow})+\sin(\alpha+\alpha_0)\sin(\Delta\Phi^{\rm on}_{\uparrow\downarrow})]\}\end{array}\right\},\tag{A24}$$

where this expression has been written in terms of the spin-up phases. This is in the form

$$N_{3\text{down}}=\left(\frac{1-P}{2}\right)N_1\{a_{3\text{down}}+b_{3\text{down}}\cos(\alpha+\alpha_0+\Delta\Phi^{\rm on}_{\rm down})\},\tag{A25}$$

where $\Delta\Phi^{\rm on}_{\rm down}$ is again the observed total spin-dependent phase for spin-down incident neutrons, such that

$$\tan\Delta\Phi^{\rm on}_{\rm down}=\frac{-\sqrt{(1-f_{\rm I})(1-f_{\rm II})}\sin\Delta\Phi^{\rm on}_{\uparrow\uparrow}-\sqrt{(1+f_{\rm I})(1+f_{\rm II})}\sin\Delta\Phi^{\rm on}_{\uparrow\downarrow}}{\sqrt{(1-f_{\rm I})(1-f_{\rm II})}\cos\Delta\Phi^{\rm on}_{\uparrow\uparrow}+\sqrt{(1+f_{\rm I})(1+f_{\rm II})}\cos\Delta\Phi^{\rm on}_{\uparrow\downarrow}}=-\tan\Delta\Phi^{\rm on}_{\rm up}=\tan(-\Delta\Phi^{\rm on}_{\rm up}),\tag{A26}$$

i.e., $\Delta\Phi^{\rm on}_{\rm down}=-\Delta\Phi^{\rm on}_{\rm up}$, as expected. Therefore, from Eqs. (A17) and (A24), the observed total spin-dependent phase shift $\Delta\Phi^{\rm on}_{\rm tot}$ of an interferogram, with a fraction $(1+P)/2$ spin-up incident neutrons and a fraction $(1-P)/2$ spin-down incident neutrons, is given by the spin-dependent phases $\Delta\Phi^{\rm on}_{\uparrow\uparrow}$ and $\Delta\Phi^{\rm on}_{\uparrow\downarrow}$ of interest by

$$\tan\Delta\Phi^{\rm on}_{\rm tot}=P\,\frac{\sqrt{(1-f_{\rm I})(1-f_{\rm II})}\sin\Delta\Phi^{\rm on}_{\uparrow\uparrow}+\sqrt{(1+f_{\rm I})(1+f_{\rm II})}\sin\Delta\Phi^{\rm on}_{\uparrow\downarrow}}{\sqrt{(1-f_{\rm I})(1-f_{\rm II})}\cos\Delta\Phi^{\rm on}_{\uparrow\uparrow}+\sqrt{(1+f_{\rm I})(1+f_{\rm II})}\cos\Delta\Phi^{\rm on}_{\uparrow\downarrow}}.\tag{A27}$$

For the case when there is no current to the spin flippers, the expression is much simpler. This corresponds to the neutron precessing about the guide field along the entire path, that is

$$\Delta\Phi^{\rm off}_{\rm up}=-\Delta\Phi^{\rm off}_{\rm down}=\Delta\phi^0_{A+B}+\Delta\phi^0_{C+D},\tag{A28}$$

where the phase accumulated by the spin-up neutrons is the negative of that accumulated by spin-down neutrons:

$$\Delta\phi^0_{A+B}=\Delta\phi_A(\Delta\beta/2)+\Delta\phi^{\rm off}_B(\Delta\beta/2)\tag{A29}$$

is the phase accumulated from the first interferometer blade to the middle of the spin-flipper, and, similarly,

$$\Delta\phi^0_{C+D}=\Delta\phi_D(\Delta\beta/2)+\Delta\phi^{\rm off}_C(\Delta\beta/2)\tag{A30}$$

is the phase for the remainder of the path to the last blade. $\Delta\phi^0_A$ and $\Delta\phi^0_D$, except for small changes due to off-center rotation as a function of $\Delta\beta/2$, are constant. Again, from Eq. (24),

$$\tan\Delta\Phi^{\rm off}_{\rm tot}=P\,\tan(\Delta\phi^0_A+\Delta\phi^0_D).\tag{A31}$$

The difference between $\Delta\Phi^{\rm on}_{\rm tot}$ obtained from Eq. (A27) and $\Delta\Phi^{\rm off}_{\rm tot}$, obtained from Eq. (A31), is $\Delta\gamma$ of Eq. (19), the measured phase difference between the on and off interferograms to be fit as a function of $\Delta\beta$.

Geometric phase

The procedure goes as follows: for the geometric phase measurements, the expressions

$$\Delta\Phi^{\rm on}_{\uparrow\uparrow}(\Delta\beta)=\Delta\phi_A(\Delta\beta)+\Delta\phi_D(\Delta\beta)+\Delta\chi^{\rm on}_{\uparrow}(\Delta\beta)$$
$$=\Delta\phi^0_A-\Delta\phi^{\rm off}_B(\Delta\beta)+\Delta\phi^0_D-\Delta\phi^{\rm off}_C(\Delta\beta)$$
$$+\Delta\chi^{\rm on}_{\uparrow}(\Delta\beta)\tag{A32}$$

and

$$\Delta\Phi^{\rm on}_{\uparrow\downarrow}(\Delta\beta)=\Delta\phi_A(\Delta\beta)-\Delta\phi_D(\Delta\beta)-s_{\Delta\beta}\Delta\beta+\Delta\chi^{\rm on}_{\downarrow}(\Delta\beta)$$
$$=\Delta\phi^0_A-\Delta\phi^{\rm off}_B(\Delta\beta)-\Delta\phi^0_D+\Delta\phi^{\rm off}_C(\Delta\beta)$$
$$-s_{\Delta\beta}\Delta\beta+\Delta\chi^{\rm on}_{\downarrow}(\Delta\beta),\tag{A33}$$

representing the spin-dependent phase shifts, contain constants $\Delta\phi^0_A$, $\Delta\phi^0_D$, and $s_{\Delta\beta}$, and measurables $\Delta\chi^{\rm on}_{\uparrow}(\Delta\beta)$, $\Delta\chi^{\rm on}_{\downarrow}(\Delta\beta)$,

$$\Delta\phi^{\rm off}_B(\Delta\beta)=2\left(\frac{\mu B^{\rm II}_{ZB}}{\hbar v}-\frac{\mu B^{\rm I}_{ZB}}{\hbar v}\right)W'\tag{A34}$$

and

$$\Delta\phi^{\rm off}_C(\Delta\beta)=2\left(\frac{\mu B^{\rm II}_{ZC}}{\hbar v}-\frac{\mu B^{\rm I}_{ZC}}{\hbar v}\right)W',\tag{A35}$$

where $W'=W/\cos(\Delta\beta/2)$.

The values for $\phi_B(\Delta\beta)$ and $\phi_C(\Delta\beta)$, the phase shift across an individual coil of the dual flipper used in $\Delta\chi^{\rm on}_{\uparrow}(\Delta\beta)$ and $\Delta\chi^{\rm on}_{\downarrow}(\Delta\beta)$ of Eqs. (A11) and (A12), are given by

$$\phi_B(\Delta\beta)=2\left(\frac{\mu B_B}{\hbar v}\right)W'\tag{A36}$$

and

$$\phi_C(\Delta\beta)=2\left(\frac{\mu B_C}{\hbar v}\right)W'. \tag{A37}$$

From Eq. (16),

$$1_{\downarrow}=\frac{f_1P+1}{2}\,I_0 \tag{A38}$$

represents the intensity of spin-down neutrons from the incident intensity, where f_1, flipper F_1's efficiency, is given by Eq. (A8) which is a function of ϕ_B and ϕ_C. ϕ_B and ϕ_C, in turn, depend on the total magnetic field [Eq. (A5)]

$$B=\sqrt{B_Z^2+B_{y'}^2}=\sqrt{B_Z^2+(gI_{F_1})^2}, \tag{A39}$$

where I_{F_1} is the flipper current, and g is a proportionality constant determined from the measured value of the flipper coil field. Thus

$$\phi(\Delta\beta)=\left(\frac{2\mu\sqrt{B_Z^2+(gI_{F_1})^2}W'}{\hbar v}\right). \tag{A40}$$

The value of the constant $(2\mu W/\hbar v)$, was determined experimentally from a fit to the F_1 efficiency scan of Fig. 16(a) plotted as a function of I_{F_1}. As already explained, optimization of the flipper efficiency could only be performed for F_1; the results were assumed to be identical for F_2.

A simple linear regression to the geometric phase data of Fig. 11, as a function of $\Delta\beta$, has a slope of -1.36 ± 0.04. A three parameter fit for $\Delta\phi_A^0$, $\Delta\phi_D^0$, and $s_{\Delta\beta}$, based on Eqs. (A27) and (A31), which corrects for incident polarization and nonperfect spin flipping, gives -1.23 ± 0.03 for the slope of the data, $s_{\Delta\beta}$. A fit using these parameters is shown in Fig. 11. According to Eq. (2), $\Phi_G=\Delta\beta$, then theoretically, $s_{\Delta\beta}=1$; however, in assuming that $\Delta\phi_A^0$ and $\Delta\phi_D^0$ are constants, any dynamical phase contamination will be contained in $s_{\Delta\beta}$. The consequences of this are explained in the text.

Dynamical phase

For the dynamical phase data as a function of translation along the beam path δx, the spin-dependent phase shift expressions have the forms

$$\begin{aligned}\Delta\Phi_{\uparrow\uparrow}^{\rm on}(\delta x)&=\Delta\phi_A(\delta x)+\Delta\phi_D(\delta x)+\Delta\chi_{\uparrow}^{\rm on}(\delta x,\Delta\beta=0)\\&=\Delta\phi_A^0-\Delta\phi_B^{\rm off}(\delta x,\Delta\beta=0)+s_{\delta x}\delta x+\Delta\phi_D^0-\Delta\phi_C^{\rm off}(\delta x,\Delta\beta=0)-s_{\delta x}\delta x+\Delta\chi_{\uparrow}^{\rm on}(\delta x,\Delta\beta=0)\\&=\Delta\phi_A^0-\Delta\phi_B^{\rm off}(\delta x,\Delta\beta=0)+\Delta\phi_D^0-\Delta\phi_C^{\rm off}(\delta x,\Delta\beta=0)+\delta\chi_{\uparrow}^{\rm on}(\delta x,\Delta\beta=0)\end{aligned} \tag{A41}$$

and

$$\begin{aligned}\Delta\Phi_{\uparrow\downarrow}^{\rm on}(\delta x)&=\Delta\phi_A(\delta x)-\Delta\phi_D(\delta x)+\Delta\chi_{\downarrow}^{\rm on}(\delta x,\Delta\beta=0)\\&=\Delta\phi_A^0-\Delta\phi_B^{\rm off}(\delta x,\Delta\beta=0)+s_{\delta x}\delta x-\Delta\phi_D^0+\Delta\phi_C^{\rm off}(\delta x,\Delta\beta=0)+s_{\delta x}\delta x+\Delta\chi_{\downarrow}^{\rm on}(\delta x,\Delta\beta=0)\\&=\Delta\phi_A^0-\Delta\phi_B^{\rm off}(\delta x,\Delta\beta=0)-\Delta\phi_D^0+\Delta\phi_C^{\rm off}(\delta x,\Delta\beta=0)+2s_{\delta x}\delta x+\Delta\chi_{\downarrow}^{\rm on}(\delta x,\Delta\beta=0)\,.\end{aligned} \tag{A42}$$

Again, $\Delta\phi_A^0$, $\Delta\phi_D^0$, and $s_{\delta x}$ are constants and $\Delta\chi_{\uparrow}^{\rm on}(\delta x,\Delta\beta=0)$, $\Delta\chi_{\downarrow}^{\rm on}(\delta x,\Delta\beta=0)$,

$$\Delta\phi_B^{\rm off}(\delta x,\Delta\beta=0)=\left[\frac{\mu B_B^{\rm II}(\delta x)}{\hbar v}-\frac{\mu B_B^{\rm I}(\delta x)}{\hbar v}\right]W \tag{A43}$$

and

$$\Delta\phi_C^{\rm off}(\delta x,\Delta\beta=0)=\left[\frac{\mu B_C^{\rm II}(\delta x)}{\hbar v}-\frac{\mu B_C^{\rm I}(\delta x)}{\hbar v}\right]W \tag{A44}$$

are based on measured values. A plot of the Helmholtz coils' field strength $B_0\hat{\mathbf{z}}$, as a function of position inside the interferometer, is shown in Fig. 17. It is these values that are used in the equations for $\Delta\phi_B^{\rm off}$, $\Delta\phi_C^{\rm off}$, ϕ_B, and ϕ_C. A three-parameter fit is made for each of the two cases, translations along paths I and II. Results of these fits are shown in Figs. 14 and 15, and give $s_{\delta x\rm I}=-19.4\pm0.5°$/mm and $s_{\delta x\rm II}=18.9\pm0.4°$/mm, respectively. These results are discussed in the text.

[1] M. V. Berry, Proc. R. Soc. London, Ser. A **392**, 45 (1984); B. Simon, Phys. Rev. Lett. **51**, 2167 (1983).
[2] S. Pancharatnam, Proc. Ind. Acad. Sci. A **44**, 247 (1956).
[3] J. Samuel and R. Bhandari, Phys. Rev. Lett. **60**, 2339 (1988).
[4] A. G. Wagh and V. C. Rakhecha, Pramana, J. Phys. **41**, L479 (1993); V. C. Rakhecha and A. G. Wagh, *ibid.* **46**, 315 (1996).
[5] Y. Aharonov and J. Anandan, Phys. Rev. Lett. **58**, 1593 (1987).
[6] J. H. Hannay, J. Phys. A **18**, 221 (1985).
[7] J. Anandan, Phys. Lett. A **129**, 201 (1988); Nature (London) **360**, 307 (1992).
[8] A. Kitano, T. Yabuzaki, and T. Ogawa, Phys. Rev. Lett. **58**, 523 (1987).
[9] A. Tomita and R. Y. Chiao, Phys. Rev. Lett. **57**, 937 (1986).
[10] G. Delacrétaz, E. R. Grant, R. L. Whettan, L. Wöste, and J. W. Zwanziger, Phys. Rev. Lett. **56**, 2598 (1986).
[11] R. Tycko, Phys. Rev. Lett. **58**, 2281 (1987).
[12] T. Bitter and B. Dubbers, Phys. Rev. Lett. **59**, 251 (1987).
[13] D. J. Richardson, A. I. Kilvington, K. Green, and S. K. Lamoreaux, Phys. Rev. Lett. **61**, 2030 (1988).
[14] D. Suter, K. T. Mueller, and A. Pines, Phys. Rev. Lett. **60**, 1218 (1988).
[15] D. M. Bird and A. R. Preston, Phys. Rev. Lett. **61**, 2863 (1988).
[16] *Geometric Phases in Physics*, edited by A. Shapere and F. Wilczek (World Scientific, Singapore, 1989).
[17] A. G. Wagh and V. C. Rakhecha, Phys. Rev. A **48**, R1729 (1993); Phys. Lett. A **170**, 71 (1992).
[18] A. G. Wagh, Phys. Lett. A **146**, 369 (1990).
[19] A. G. Wagh and V. C. Rakhecha, Phys. Lett. A **148**, 17 (1990).
[20] H. J. Bernstein, Phys. Rev. Lett. **18**, 1102 (1967).
[21] Y. Aharonov and L. Susskind, Phys. Rev. **158**, 1237 (1967).
[22] H. Rauch, A. Zeilinger, G. Badurek, A. Wilfing, W. Bauspiess, and U. Bonse, Phys. Lett. A **54**, 425 (1975).
[23] S. A. Werner, R. Collela, A. W. Overhauser, and C. F. Eagen, Phys. Rev. Lett. **35**, 1053 (1975).
[24] A. G. Klein and G. I. Opat, Phys. Rev. Lett. **37**, 238 (1976).
[25] S. A. Werner and A. G. Klein, in *Methods of Experimental Physics*, edited by K. Skold and D. L. Price (Academic, New York 1986), Vol. 23, Pt. A, p. 259; A. G. Wagh and V. C. Rakhecha, Prog. Part. Nucl. Phys. **37**, 485 (1996).
[26] The phase Φ_G of Eq. (2) just equals the phase jump caused by the kink $\Delta\beta$ in the spin trajectory at the pole $|-z\rangle$ [4].
[27] A. G. Wagh and V. C. Rakhecha, Phys. Lett. A **197**, 107 (1995); **197**, 112 (1995).
[28] Equation (6), though not exact, is an excellent approximation for thermal neutrons in fields up to 400 G; see Ref. [18].
[29] A. G. Wagh, V. C. Rakhecha, J. Summhammer, G. Badurek, H. Weinfurter, B. E. Allman, H. Kaiser, K. Hamacher, D. L. Jacobson, and S. A. Werner, Phys. Rev. Lett. **78**, 755 (1997); J. Phys. Soc. Jpn. **65**, 73 (1996).
[30] A detailed description of the beam port *C* neutron interferometry facility at MURR is given in Russel Clothier's Ph.D. thesis, University of Missouri-Columbia, 1991 (unpublished).
[31] J. Summhammer, K. A. Hamacher, H. Kaiser, H. Weinfurter, D. L. Jacobson, and S. A. Werner, Phys. Rev. Lett. **75**, 3206 (1995).
[32] J. Summhammer, G. Badurek, H. Rauch, U. Kischko, and A. Zeilinger, Phys. Rev. A **27**, 2523 (1983); the effect is mentioned at the beginning of page 2529.